

# How to observe the QCD instanton/sphaleron processes at hadron colliders?

Edward Shuryak and Ismail Zahed

*Center of Nuclear Theory, Department of Physics and Astronomy,  
Stony Brook University, Stony Brook, NY 11794, USA*

---

## Abstract

The instanton/sphaleron processes involve gauge fields with changing topology, including a nonzero variation of the Chern-Simons number  $\Delta N_{CS} = \pm 1$ . In QCD such processes lead to the production of  $2N_f \Delta N_{CS}$  units of the axial charge, proportional to the number of light quark flavors  $N_f = 3$ , for  $u, d, s$ . In the electroweak theory such processes lead to the production of 12 fermions, with  $\Delta B = \Delta L = \pm 3$  units of baryon and lepton number. While this is all known for a long time, and is one of the pillars of the nonperturbative theory of the QCD vacuum, in this paper we discuss what we call a “reclined tunneling”, in which external forces are added to the tunneling processes and create certain gluonic objects with positive invariant mass. The idea to observe these objects experimentally at hadronic colliders have been proposed before, but insofar without success. Motivated by the recent CERN workshop on the topic, we review these ideas. We put forward our own suggestions, in particular to utilize a double-diffractive (Pomeron-Pomeron) collisions to this goal, which we believe maximizes the entrance factor and minimizes the backgrounds. We consider clusters of small ( $M = 3 - 10$  GeV), medium ( $M = 10 - 30$  GeV) and high  $M \sim 100$  GeV invariant masses, subsequently. Among the proposed signals are specific flavor combination of channels, originating from well-defined 6-, 8- and 10-quark-antiquark operators, as well as correlation of quark chiralities to be potentially detected via  $\Lambda$  hyperon decays.

---

## 1. Introduction

### 1.1. The instanton/sphaleron processes

In going to the mountains, one needs a reliable map and preferably from a variety of sources. Building a tunnel is expensive, so one needs to think a lot. Should it be horizontal or reclined? Where should the entrance be, and where should the exit be? As we will see shortly, all such questions also appear when we think of optimal paths producing topologically nontrivial final states in a collision.

Some of these questions have already been answered in theory decades ago, but some still require further analyses and calculations. There is a vast number of applications of instanton-induced effects in vacuum and hadronic structure. The instanton-sphaleron processes, producing certain topologically nontrivial gluonic clusters, are only seen in low-mass domain, like  $\eta_c$  decays. This paper is about possible ways to see such objects at hadron colliders, with variable masses.

One can split the expected cross section into three distinct parts: (i) tunneling action; (ii) the semiclassical prefactor; (iii) the entrance factor; and, last but not least, (iv) branching ratios into particular exclusive channels, or sequentially

$$\sigma \sim \left[ \frac{\text{entrance}}{\text{factor}} \right] \left[ \frac{\text{semiclassical}}{\text{prefactor}} \right] \left[ e^{-S_{cl}} \right] \left[ B(\text{final state}) \right] \quad (1)$$

As we show below, the classical part is well under control. The semiclassical prefactor is not yet calculated for gauge theory beyond one loop, but it was done in relevant toy models, so it can be evaluated if needed. The entrance factor is really the difficult part still in deliberation.

The produced unstable magnetic objects, generically known as “sphalerons”, explode into outgoing gluon and quark waves, which eventually “hadronize” into mesons and baryons going to the detectors. This initial part of this process is described by a solution of the classical YM equation, see section 4. Quark pair production is described by the solution of the Dirac equation in the exploding background. For all light quark flavors one has the same solution, which results in an effective 6-quark operator of the flavor composition  $(\bar{u}u)(\bar{d}d)(\bar{s}s)$  and with specific chiral properties. Its projection onto the distribution amplitudes of pertinent mesons, provides the decay probabilities to exclusive final states, e.g. for three mesons those are  $KK\pi, \pi\pi\eta, \pi\pi\eta'$ .

A further discussion of heavy  $(c, b)$  quark production is done in section 7.3. We will estimate the sphaleron scales at which such production becomes possible, and then discuss 8- and 10-fermion operators and their final states such as  $KKDD$  and  $BBD_sDK$ .

### 1.2. Double diffraction and Pomerons, glueballs and clusters

In multiple papers the instanton/sphaleron process was calculated with the assumption that it is initiated at a partonic level, gluon-gluon or quark-antiquark collisions. In this case the secondaries originated from sphalerons are imbedded in complicated  $pp$  collisions, together with many other jets and secondaries produced. The separation of the signal from backgrounds is in this case very difficult.

Perhaps the main idea first expressed in [1], is that one may avoid large backgrounds associated with min.bias  $pp$  collisions, by using double diffractive events (also known as Pomeron-Pomeron abbreviated as **PP**, distinct from  $pp$ ). We start with a brief summary of the experimental situation, before elaborating on various theoretical models.

The two early experiments of interest are WA102 [2] and WA8 [3], both of which were carried decades ago at CERN .

WA102 was driven by an idea that the **PP** processes provide a “glueball filter”, allowing to separate glueball-type hadrons from other mesons. It provided important data on the distribution over the azimuthal angle  $\phi$ , between the transverse momentum transfers to both surviving protons. The collaboration identified a certain number of scalar, pseudoscalar and tensor hadronic resonances in the invariant mass distribution. As a subsequent discussion has shown, the collaboration has indeed seen not only a scalar glueball candidate, but also a tensor  $2^+$  glueball at a mass of 2.2 GeV. Both have angular distributions in  $\phi$  completely different from those for ordinary mesons.

WA8 was focused on larger invariant masses. Unfortunately, its central detector was just a calorimeter, so no exclusive channels were studied. This collaboration reported observation of some isotropically decaying “clusters”, with a mass peaked at  $M \approx 3$  GeV, which we will discuss further in sections 6.2 and 11. They also reported non-isotropic background events with masses  $M = 5 - 20$  GeV.

The revival of the diffractive field at the LHC has begun relatively recently. The Atlas Forward Proton (AFP) detector was installed and ran, but it is focused on producing systems with very large mass in the range of hundreds of GeVs. In our understanding, ATLAS ALFA forward detectors were designed to measure forward elastic scatterings. On the other hand, the CMS-TOTEM collaborations, working together, have addressed soft **PP** reactions, and recently reported soft exclusive  $\pi^+\pi^-$  data [4]. They focused on small invariant mass region  $M(\pi^+\pi^-) < 2$  GeV and have confirmed the production of (at least) four scalar and tensor mesons, all seen previously by WA102. From a wider perspective, apart from focusing on glueball spectroscopy, these experiments have provided important insights into the structure of the Pomeron-Pomeron-hadron vertices, and thus the structure of the Pomeron itself.

From the theory side, during the last decade there were basically two major developments:

(i) The Pomeron is defined as a virtual state, described by continuation of a glueball Regge trajectory from positive to small negative  $t$  domain, where it is observed in scattering. Note that the nearest physical state to it is the tensor  $2^{++}$  glueball. In holographic models of QCD this glueball is identified with the excitation of bulk gravitons [5, 6]. This, and other consideration, relate Pomeron exchanges with Reggeized graviton exchanges. These ideas have explained well the WA102 data production of pseudoscalar [7] and

tensor [8] glueballs. In this latter paper the  $\mathbf{PP}\text{-}2^+$  vertex used was a 3-tensor coupling deduced from the Einstein-Hilbert action of general relativity. Earlier suggestions that the Pomeron phenomenology needs some *polarization tensor* were made by the Heidelberg group, see review in [9].

(ii) From the 1970's the perturbative theory of the Pomeron was based first on two-gluon exchanges, and then developed into inclusion of ladder diagrams with gluonic rungs. This theory culminated in the famed papers [10] and is known as the BFKL Pomeron. It is successful in describing diffraction with large  $|t| > \text{few GeV}$ . Yet at small  $|t|$  (or large impact parameter  $b \sim 1/\sqrt{|t|}$ ) there is no reason to use perturbative QCD. Alternative theory for this case, based on ‘‘stringy instanton’’ solution to Nambu-Goto string exchange was developed in [11], and is known as the BKYZ Pomeron. Although the two theories start from very different descriptions, with different interpretations of the parameters, the scattering amplitude is nearly the same. The latter BKYZ version, unlike BFKL, tells when the transition in impact parameter should happen, as strings undergo Hagedorn transition.

## 2. The topological landscape

The Hilbert space of all possible gauge potentials  $A_a^\mu(x)$  is the manifold over which we need to integrate the Feynman path integral. Of course, we would not discuss infinite-dimensional maps, and focus on two main variables, for all static (3-dimensional and purely magnetic) configurations of the lowest energy, consistent with the value of those coordinates. One of the coordinates is the topological Chern-Simons number

$$N_{CS} \equiv \frac{\epsilon^{\alpha\beta\gamma}}{16\pi^2} \int d^3x \left( A_\alpha^a \partial_\beta A_\gamma^a + \frac{1}{3} \epsilon^{abc} A_\alpha^a A_\beta^b A_\gamma^c \right) \quad (2)$$

which is integer for pure gauge configurations, at which the energy is zero. Those points will be referred to as ‘‘valley minima’’. The other coordinate is the mean square radius of the magnetic field strength squared

$$\rho^2 \equiv \frac{\int d^3x \vec{x}^2 \vec{B}^2}{\int d^3x \vec{B}^2} \quad (3)$$

Without fixing it, there is no minimal energy, as simple rescaling can change it.

By the ‘‘topological landscape’’ we mean the 2-dimensional profile of the minimal energy  $U_{\min}(N_{CS}, \rho)$  of gauge field configurations with those two coordinates fixed. For pure gauge theory, such minimal energy configurations themselves, are known as the ‘‘sphaleron path’’: as changing  $N_{CS}$  from one integer to the next we are leading from one topological valley to another, keeping minimal energy at any point. Those were derived by Carter, Ostrovsy and one of us [12] by two different methods. The one related with the instanton/sphaleron process will be discussed in the next section. The second method is minimization with two Lagrange multipliers times two conditions, (2) and (3). The minimal energy along the path was obtained in a parametric form

$$\begin{aligned} U_{\min}(\kappa, \rho) &= (1 - \kappa^2)^2 \frac{3\pi^2}{g^2 \rho} \\ N_{CS}(\kappa) &= \frac{1}{4} \text{sign}(\kappa) (1 - |\kappa|)^2 (2 + |\kappa|) \end{aligned} \quad (4)$$

The result shows a profile of the ‘‘topological mountain’’ of the gauge theory, see Fig. 1, also known as ‘‘the sphaleron path’’. Its maximum, at  $\kappa = 0$ , has  $N_{CS} = \frac{1}{2}$  and its energy is known as the *sphaleron mass*

$$M_{sph} = U_{\min}\left(\frac{1}{2}, \rho\right) = \frac{3\pi^2}{g^2 \rho} \quad (5)$$

When the momentum scale  $1/\rho$  is high, the gauge fields are very strong and one can neglect the ‘‘vacuum structure’’ effects and keep only the classical Yang-Mills equation. Of course, this equation is scale-invariant, and therefore  $U_{\min} \sim 1/\rho$ . However, if  $1/\rho$  is small enough, one can no longer neglect vacuum effects.

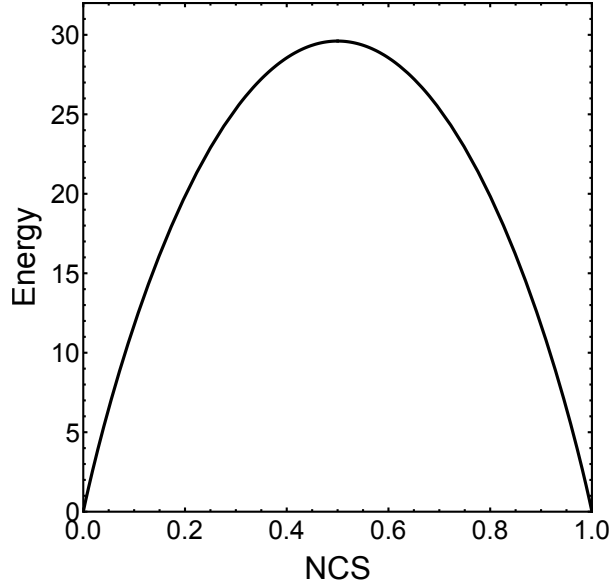


Figure 1: The potential energy  $U_{\min}(N_{CS}, \rho)$  (in units of  $1/g^2\rho$ ) versus the Chern-Simons number  $N_{CS}$  for the “sphaleron path” between  $N_{CS} = 0$  and  $N_{CS} = 1$ .

In the electroweak theory these “vacuum effects” are described by the Higgs field  $\phi$ . The scale is set by its VEV  $v = \langle \phi \rangle \approx 246$  GeV. Ignoring first the Weinberg angle and using variational methods, Klinkhamer and Manton [13] have included the Higgs field and solved the YM+scalar equations. They observed that the Higgs field must vanish at the origin  $r = 0$  to keep the topology of the gauge field intact, and therefore the sphaleron is a “semi-empty bag” inside the Higgs vacuum. This adds some energy: e.g. the leading term at large  $\rho$  proportional to the bag volume and the highest power of the Higgs VEV

$$U_{\text{Higgs}} \sim \rho^3 v^4$$

The  $1/\rho$  gauge term plus Higgs terms with positive powers of the size leads to a minimum at a certain  $\rho^*$ , which fixes the configuration completely. The mass of the electroweak sphaleron is found to be about 9 TeV. Thus, going from one topological valley of the electroweak theory to another, one needs at least that much energy. All of that was clear since 1984.

Proceeding to our main object of interest, the sphaleron path in QCD, we note that the QCD vacuum also has a rather complicated vacuum structure, with nontrivial VEVs of various operators (known as “vacuum condensates”). There are lattice data and models of the QCD vacuum structure, that provides some understanding of the topological landscape at large  $\rho$ . It will be discussed below, and here we just state that they also force the minimal energy  $U_{\min}(1/2, \rho)$  to start growing at large  $\rho$ , also producing some optimal size  $\rho^*$ .

### 3. The tunneling paths

The first “tunneling path” was the original BPST instanton discovered in 1975. It is the solution of the Euclidean YM equation. In terms of the landscape illustrated in Fig. 1, it is a horizontal path, at energy zero, leading directly from the bottom of one valley to the bottom of the next one. The tunneling amplitude along it is  $\sim \exp(-8\pi^2/g^2)$ , given by the action of the instanton.

Many of the discussions on how to improve the tunneling path, including the final state gluon radiation, were the subject of complicated technical papers in the late 1980’s. We would not describe them, but

just state that Khoze and Ringwald [14], as well as Verbaarschot and Shuryak [15], have suggested that 4-dimensional configurations describing the *optimal* instanton-antiinstanton  $I\bar{I}$  also provide the *optimal path for sphaleron production*. Since then, most calculations follow this idea.

Before going to the details, let us explain why it is the case, following important insights from [12, 16, 17]. The  $I\bar{I}$  configuration is schematically shown in the upper plot of Fig. 2. The shaded circles indicate regions where the instanton and antiinstanton fields are strong. In one of them, the fields are (close to) self-dual  $\vec{E} = \vec{B}$ , and in the other anti-self-dual  $\vec{E} = -\vec{B}$ . If both have the same sizes and color orientations, symmetry of the plot suggest that the electric field  $\vec{E}$  changes sign at  $t \rightarrow -t$ , and is therefore zero at  $t = 0$ . The 3-dimensional plane in the middle of the plot must contain a pure magnetic configuration, corresponding to semiclassical “turning points” where the momentum vanishes. At such points the paths go from a tunneling process in Euclidean time to a “real life” process in Minkowski space.

So, the  $t = 0$  plane is nothing else but the “unitarity cut”, familiar from perturbative Feynman diagrams. The object on it *is* the object produced. the two halves of the  $I\bar{I}$  4-dimensional configurations are the amplitude and the conjugated amplitude. They describe the probability to produce this object. Any discussion of the multi-gluon production, with the complicated interferences between them, are not needed at all: what is produced is this classical magnetic object.

Now, why is it that this tunneling path is better than the original instanton (or  $R \rightarrow \infty$  limit)? It may be confusing at first glance, since the  $I\bar{I}$  configurations are *not* solutions of the YM equations. They are tunnels *included upward* as indicated by the arrows in the lower plot of Fig. 2. Indeed, to go uphill an external force is needed: but on those paths the action is reduced! (As we will see, roughly by a factor 2, or many decades in the rates.)

Instead of ending at the bottom of the valley, these paths end at some points on the slopes (indicated by red and green balls). After the corresponding magnetic objects are born, they roll down (explode) classically. Their action is real,  $|\exp(iS)| = 1$ , and therefore their decays have probability one. Whatever decays they have, it does not affect the cross section.

As it is clear from the lower plot of Fig. 2, for small  $R$  the instanton and antiinstanton nearly annihilate each other and their combined action can be reduced all the way to zero. If the product has  $N_{CS} < 1/2$ , it will not roll to the second valley, but return to the original one. The anomaly relation then would indicate no fermionic transitions. In summary: there exist *topologically trivial* and *topologically nontrivial* tunnelling paths! One cannot economize more than (roughly) *half* of the instanton+antiinstanton action.

The issue of instanton-antiinstanton ( $I\bar{I}$ ) interactions has its own long history. When instanton and antiinstanton are well separated, the simple “sum ansatz” gives twice the action, but what if the distance between them is comparable to their size? One can invent many arbitrary interpolations.

The idea in [18] was to “follow the force” using  $\partial S/\partial x(\tau)$ . In this way one gets a set of configurations, which are action minima for infinitely many perturbations, except along one direction – the set itself. One of us has independently generated this set numerically [19] for the double well <sup>1</sup>. Yung [20] proposed the “Yung ansatz” solving the streamline equation at large  $R$ .

For gauge theory instantons the problem looked more complicated. First of all, even a sum ansatz could not be used, as special cancellations near the centers (in singular gauge) were spoiled as the field strength gets singular. For this purpose a “ratio ansatz” was developed to cure this. Furthermore, it looked that the interaction should depend on at least 3 variables,  $\rho_I, \rho_A, R$ , even for identical color orientations. Verbaarschot [21] however, noticed that since the classical YM theory has conformal symmetry, the answer

---

<sup>1</sup>We did not know then that in mathematics our “streamlines” were known in complex analysis as “Lefschitz thimbles”, special lines connecting saddles in the complex plane.

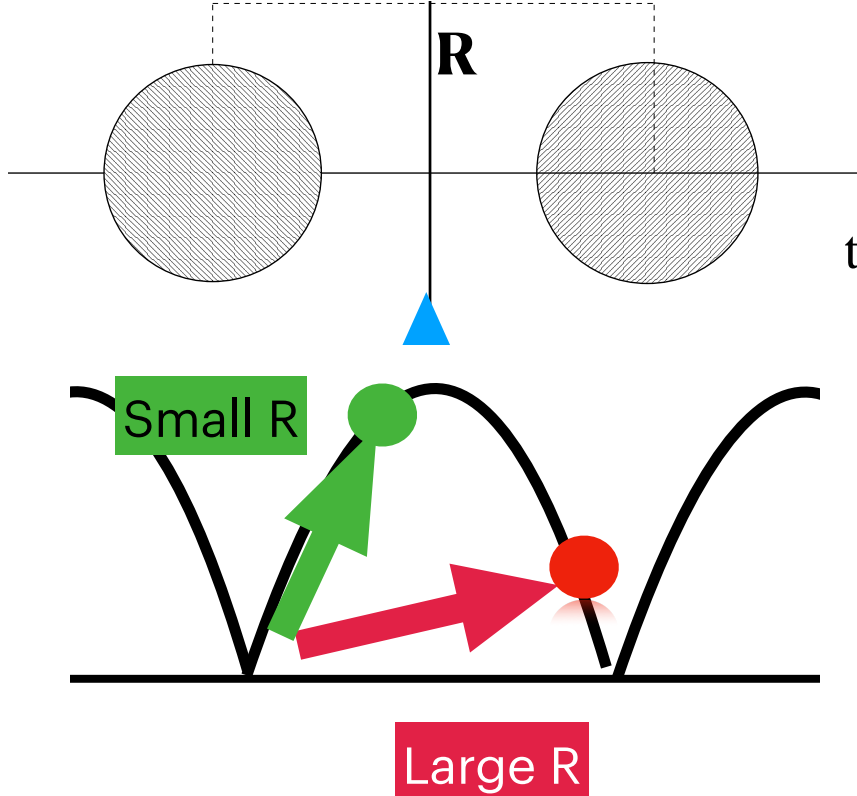


Figure 2: The upper plot shows a schematic picture of the instanton-antiinstanton configuration. The horizontal axis is (Euclidean) time  $t$ , and  $R$  is the distance between their centers. The blue triangle indicates  $t = 0$ , a 3-dimensional hyper-surface in which the produced magnetic object resides. The lower plot with the red arrow, refers to the “reclined tunnel” corresponding to large  $R$ . The green arrow on the left indicates tunneling for small  $R$ , with a Chern-Simons number of the produced object  $N_{CS} < 1/2$ . For this last case, the classical explosion returns the system to the original valley.

should depend on their single conformal-invariant combination <sup>2</sup>

$$\frac{R^2 + (\rho_1^2 - \rho_2^2)^2}{\rho_1 \rho_2} \quad (6)$$

Using an appropriate conformal map, the antiinstanton was set inside the instanton, and the problem was mapped onto the double-well potential. As a general surprise, Verbaarschot’s configurations happen to be described rather accurately by Yung ansatz, not only at large  $R$  as was originally claimed, but in fact all the way to  $R \rightarrow 0$  <sup>3</sup>.

To complete the story, let us mention that in [12] it was shown that the “streamline”  $I\bar{I}$  configurations, well approximated by Yung ansatz, do indeed describe  $U_{\min}(N_{CS}, \rho)$  in complete agreement with the constrained minimization already shown in Fig 1. The parameter  $\kappa$  is played by the relative separation  $R$ .

#### 4. Classically exploding sphalerons

Both static and time-dependent exploding solutions for the pure-gauge sphaleron have been originally discussed by Carter, Ostrovsky and Shuryak (COS) [12]. A simpler derivation, to be used below, has been

<sup>2</sup>Many years later, it was realized that this is a geodesic distance between two points in  $AdS_5$  space, if  $\rho$  is the extra coordinate.

<sup>3</sup>The formula itself remained complicated, and nobody – Yung included – suspected it to be a pure gauge, with zero field strength!

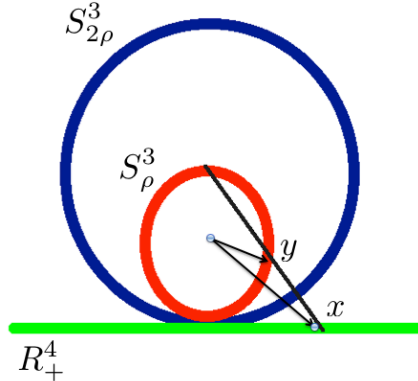


Figure 3: The inversion of the 3-sphere  $S^3_\rho$  of radius  $\rho$  onto the upper part of Minkowski space with  $t \geq 0$  or  $R^4_+$ , through the 3-sphere  $S^3_{2\rho}$  of radius  $2\rho$ .

subsequently given in [22]. The technique relies on an *off-center conformal transformation* of the  $O(4)$  symmetric Euclidean instanton solution, which is analytically continued to Minkowski space-time. However, the chief focus of that work [22] was the description of the fermion production.

The original  $O(4)$ -symmetric solution is given by the following ansatz

$$gA_\mu^a = \eta_{a\mu\nu} \partial_\nu F(y), \quad F(y) = 2 \int_0^{\xi(y)} d\xi' f(\xi') \quad (7)$$

with  $\xi = \log(y^2/\rho^2)$  and  $\eta$  the 't Hooft symbol. Upon substitution of the gauge fields in the gauge Lagrangian one finds the effective action for  $f(\xi)$

$$S_{\text{eff}} = \int d\xi \left[ \frac{\dot{f}^2}{2} + 2f^2(1-f)^2 \right] \quad (8)$$

corresponding to the motion of a particle in a double-well potential. In the Euclidean formulation, as written, the effective potential is inverted

$$V_E = -2f^2(1-f)^2 \quad (9)$$

and the corresponding solution is the well known BPST instanton, a path connecting the two maxima of  $V_E$ , at  $f = 0, f = 1$ . Any other solution of the equation of motion following from  $S_{\text{eff}}$  obviously generalizes to a solution of the Yang-Mills equations for  $A_\mu^a(x)$  as well. The sphaleron itself is the static solution at the top of the potential between the minima  $f = -1/2$ .

The next step is to perform an off-center conformal transformation as illustrated in Fig. 3

$$(x+a)_\mu = \frac{2\rho^2}{(y+a)^2} (y+a)_\mu \quad (10)$$

with  $a_\mu = (0, 0, 0, \rho)$ . It changes the original spherically symmetric solution to a solution of Yang-Mills equation depending on new coordinates  $x_\mu$ , with a separate dependences on the time  $x_4$  and the 3-dimensional radius  $r = \sqrt{x_1^2 + x_2^2 + x_3^2}$ .

The last step is the analytic continuation to Minkowski time  $t$ , via  $x_4 \rightarrow it$ . The original parameter  $\xi$  in terms of these Minkowskian coordinates, which we still call  $x_\mu$ , has the form

$$\xi = \frac{1}{2} \log \left( \frac{y^2}{\rho^2} \right) = \frac{1}{2} \log \left( \frac{(t+i\rho)^2 - r^2}{(t-i\rho)^2 - r^2} \right) \quad (11)$$

which is purely imaginary. To avoid carrying the extra  $i$ , we use the real combination

$$\xi_E \rightarrow -i\xi_M = \arctan \left( \frac{2\rho t}{t^2 - r^2 - \rho^2} \right) \quad (12)$$

and in what follows we will drop the suffix  $E$ . Switching from imaginary to real  $\xi$ , corresponds to switching from the Euclidean to Minkowski spacetime solution. It changes the sign of the acceleration, or the sign of the effective potential  $V_M = -V_E$ , to that of the normal double-well problem.

The solution of the equation of motion is given in [22]<sup>4</sup>

$$f(\xi) = \frac{1}{2} \left[ 1 - \sqrt{1 + \sqrt{2\epsilon}} \operatorname{dn} \left( \sqrt{1 + \sqrt{2\epsilon}} (\xi - K), \frac{1}{\sqrt{m}} \right) \right] \quad (13)$$

where  $\operatorname{dn}(z, k)$  is one of the elliptic Jacobi functions,  $2\epsilon = E/E_s$ ,  $2m = 1 + 1/\sqrt{2\epsilon}$ ,  $E = V(f_{\text{in}})$  is the conserved energy of the mechanical system normalized to that of the sphaleron  $E_s = V(f = 1/2) = 1/8$ . (13) reduces to the SO(4) solution derived by Luscher [23], and the hypertorus solution obtained by Schechter [24]. Since starting from exactly the maximum takes a divergent rolling time, we will start from the nearby turning point with

$$f(0) = f_{\text{in}} = \frac{1}{2} - \tau, \quad f'(0) = 0 \quad (14)$$

where a small displacement  $\tau$  ensures that the ‘‘rolling downhill’’ from the maximum takes a finite time and that the half-period  $K$  – given by an elliptic integral – in the expression is not divergent. In the plots below we will use  $\kappa = 0.01$ , but the results dependent on its value very weakly.

The solution above describes a particle tumbling periodically between two turning points, and so the expression above defines a periodic function for all  $\xi$ . However, as it is clear from (12), for our particular application the only relevant domain is  $\xi \in [-\pi/2, \pi/2]$ . Using the first 3 nonzero terms of its Taylor expansion

$$f \approx 0.4929 - 0.00706 \xi^2 - 0.0011 \xi^4 - 0.000078 \xi^6 \quad (15)$$

we find a parametrization with an accuracy of  $10^{-5}$ , obviously invisible in the plot and more than enough for our considerations.

The gauge potential has the form [22]

$$gA_4^a = -f(\xi) \frac{8t\rho x_a}{[(t-i\rho)^2 - r^2][(t+i\rho)^2 - r^2]} \quad (16)$$

$$gA_i^a = 4\rho f(\xi) \frac{\delta_{ai}(t^2 - r^2 + \rho^2) + 2\rho\epsilon_{aij}x_j + 2x_ix_a}{[(t-i\rho)^2 - r^2][(t+i\rho)^2 - r^2]}$$

which is manifestly real. From those potentials we generate rather lengthy expressions for the electric and magnetic fields, and eventually for CP-violating operators, using Mathematica.

Note that the sphaleron solution corresponds to  $t = 0$  or static, which is a pure magnetic solution with  $gA_4^a = 0$ . The magnetic field squared is spherically symmetric and simple

$$\vec{B}^2 = \frac{96\rho^4}{(\rho^2 + r^2)^4} \quad (17)$$

---

<sup>4</sup>There was a misprint in the index of this expression in the original paper.



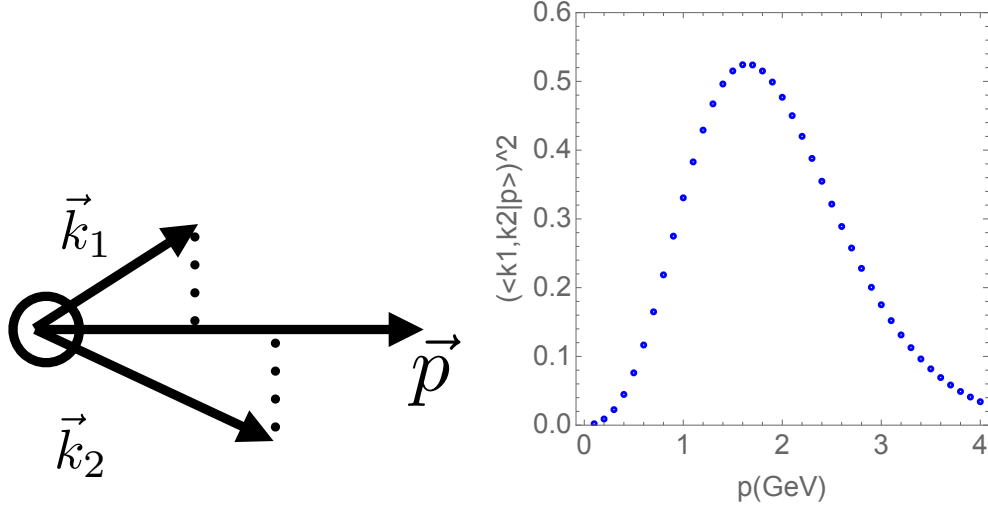


Figure 4: Upper plot: kinematics for two emerging quarks with momenta  $\vec{k}_{1,2}$  from an exploding sphaleron, fusing into a meson of momentum  $\vec{p}$ ; Lower plot: squared projection of outgoing quark waves into a mesonic distribution amplitude with momentum  $p$  (GeV).

The ensuing explosion starting from the sphaleron at  $t = 0$ , we describe using the YM equations. This is justified only if the sphaleron size is sufficiently small  $\rho \ll \rho_{\max}$  compared to the maximal size defined by the vacuum effects. If  $\rho v \sim 1$  (where  $v$  is the Higgs VEV in the electroweak theory, or the dual Higgs VEV in QCD), the equations get modified by additional terms with scalar fields.

It is known for a long time, that the Adler-Bell-Jackiw chiral anomaly relates the divergence of the axial current to the topological charge  $Q$ . Also divergence of the Chern-Simons topological current is proportional to it. As a result, their combination is conserved, and changes in the axial charge and Chern-Simons number are locked

$$\Delta Q_5 = (2N_f)\Delta N_{CS} \quad (18)$$

where  $N_f = 3$  is the number of light quark flavors.

In agreement with these general arguments, we have constructed in [22] the analytical solutions of the Dirac equation in the field of exploding sphalerons. As a function of time, one can see how quarks are accelerated from the lower Dirac sea to the physical continuum of positive energies. The spectrum of outgoing quarks has a simple form

$$\frac{dN}{dk} = 4\pi k^2 |\psi(k)|^2 = \rho(2k\rho)^2 e^{-2k\rho} \quad (19)$$

which is similar to a Planckian spectrum with an effective temperature  $T_{\text{eff}} = 1/(2\rho)$ . For the maximum value set by the vacuum instanton size distribution  $\rho_{\max} \approx 0.3 \text{ fm} \approx 1/(600 \text{ MeV})$ , the effective temperature is 300 MeV. The mean momentum is

$$\langle k \rangle = \frac{3}{2\rho} \sim 900 \text{ MeV}$$

A simple quantum estimate of the production amplitude, follows from the projection of the emerging quarks onto the distribution amplitudes (DAs) of the outgoing mesons at any momenta as illustrated in Fig.4 (upper). More specifically, we have

$$\langle \vec{k}_1, \vec{k}_2 | \vec{p} \rangle \sim \int dk_{1\perp}^2 dk_{1l} dk_{1\perp}^2 dk_{2l} \psi(\vec{k}_1) \psi(\vec{k}_2) f(p_{\perp}^2) \varphi(x = k_{1l}/P) \delta(k_{1\perp}^2 - p_{\perp}^2) \delta(k_{2\perp}^2 - p_{\perp}^2) \delta(k_{1l} + k_{2l} - P) \quad (20)$$

where  $\psi(k)$  is the outgoing quark wave (19), and the functions  $\varphi(x)f(p_{\perp}^2)$  are the DAs of the corresponding mesons with longitudinal fraction ( $x$ ) and transverse ( $p_{\perp}$ ) momenta. For simplicity, we take a Gaussian

$f(p_\perp) \sim \exp(-\text{const} * p_\perp^2)$  and a flat  $\varphi(x) = 1$  which approximate well say a pion. The squared projection for a sphaleron of size  $\rho = 0.3 \text{ fm} = 1/(0.6 \text{ GeV})$  is shown in the lower plot, as a function of the outgoing meson momentum  $p_\perp$ .

(Note that in this estimate we ignored all the other particles produced. In reality the total mass of the cluster puts its own kinematical restrictions. For example, for three-meson decay modes to be discussed, the tail at large momenta is cutoff above  $M/3$ .)

## 5. The instanton size distribution in the QCD vacuum

By now, the subject of instantons in the QCD vacuum is well established and broad, and clearly goes beyond the scope of this review. For us, the only relevant issue is the instanton size distribution  $dn/d\rho$  in the vacuum. It has been evaluated in various models and on the lattice. For definiteness we use the lattice results from [25]. The average size was found to be  $\langle\rho\rangle \approx 0.30 \pm 0.01 \text{ fm}$ , a bit smaller than in the ILM. The mean distance was found instead to be  $0.61 \pm 0.02 \text{ fm}$ . The data on the instanton size distribution are shown in Fig.5. (The figure is taken from [26] and the lattice data from Hasenfratz et al [25]). The left plot shows the size distribution itself. Recall that the semiclassical theory predicts it to be  $dn/d\rho \sim \rho^{b-5}$  at small sizes, with  $b = 11N_c/3 = 11$  for pure gauge  $N_c = 3$  theory. The right plot – in which this power is taken out – is constant at small  $\rho$ , which agrees with the semiclassical prediction.

The other feature is a peak at  $\rho \approx 0.3 \text{ fm}$  – the value first proposed phenomenologically in [27], decades before the lattice data. The peak is due to a suppression at large sizes. Trying to understand its origin, one may factor out all known effects. The right plot shows that after this is done, a rather simple suppression factor  $\sim \exp(-\text{const} * \rho^2)$  describes it well, for about 3 decades. What is the physical origin of this suppression?

There are two answers to that question, which are perhaps “Poisson dual” to each other [28]. The first is that it is due to the mutual repulsion between an instanton and the rest of the instanton-antiinstanton ensemble. (It is described in the mean field approximation and numerically, see the review [29]).

Another one, proposed in [26], is that the coefficient is proportional to the dual magnetic condensate, that of Bose-condensed monopoles. It has been further argued there that it can be related to the string tension  $\sigma$ , so that the suppression factor should be

$$\frac{dn}{d\rho} = \left(\frac{dn}{d\rho}\right)_{\text{semiclassical}} \exp[-2\pi\sigma\rho^2] \quad (21)$$

where the Higgs VEV is traded for the string tension  $\sigma$  via the dual Higgs model of confinement. If this idea is correct, this suppression factor should be missing at  $T > T_c$ , in which the dual magnetic condensate is absent. However, in this regime, quantum/thermal fluctuations generate at high  $T$  a similar factor [30]

$$\frac{dn}{d\rho} = \left(\frac{dn}{d\rho}\right)_{T=0} \exp[-(2N_c + \frac{N_f}{3})(\pi\rho T)^2] \quad (22)$$

related to the scattering of the quarks and gluons of the quark-gluon-plasma (QGP) on the instanton [31]. Empirically, the suppression factor at all temperatures looks Gaussian in  $\rho$ , interpolating between those limiting regimes.

## 6. Quark flavor signatures of instanton/sphaleron process at small $M = 3 - 10 \text{ GeV}$

### 6.1. The instanton-induced glueball and $\eta_c$ decays

As emphasized earlier, the instantons are virtual paths at zero energy, playing a significant role in the theory of the QCD vacuum, for a review see e.g. [29]. Their existence has been unambiguously revealed by the cooled lattice simulations carried by many groups, e.g. Leinweber [32].

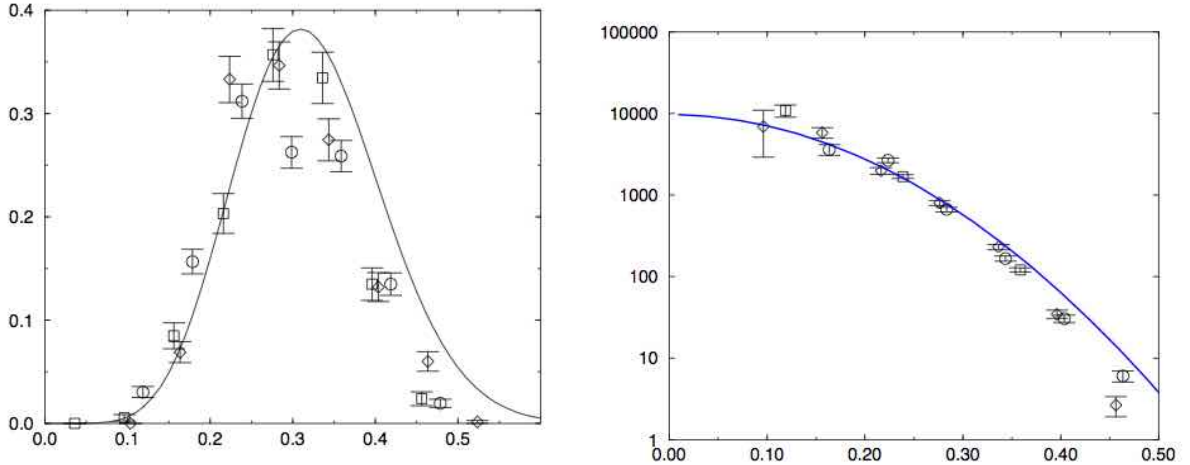


Figure 5: (left) The instanton size  $\rho$  [fm] distribution  $dn/(d\rho d^4z)$ . (right) The combination  $\rho^{-6} dn/d\rho d^4z$ , in which the main one-loop behavior drops out for  $N_c = 3, N_f = 0$ . The points are from the lattice work for this theory, with  $\beta=5.85$  (diamonds), 6.0 (squares) and 6.1 (circles). Their comparison should demonstrate that results are lattice-independent. The line corresponds to the proposed expression, see text.

The subject of this work, the instanton/sphaleron process, requires external forces able to provide the amount of energy needed for the sphaleron production. Furthermore, one should look for reactions involving gluons in combinations to which instantons are naturally coupled. Those are in scalar combinations or  $G_{\mu\nu}^2$  and pseudoscalar combinations or  $G_{\alpha\beta}G_{\gamma\delta}\epsilon^{\alpha\beta\gamma\delta}$ . In order of increasing mass, they are:

- (i) decays of a scalar glueball ( $M \approx 1.6 \text{ GeV}$ );
- (ii) decays of a pseudoscalar glueball ( $M \approx 2.5 \text{ GeV}$ );
- (iii) decays of pseudoscalar quarkonia<sup>5</sup> ( $M_{\eta_c} \approx 3 \text{ GeV}$ )

The main idea of this work is that gluon-gluon or (especially) Pomeron-Pomeron collisions also couple to such operators by fusion, and through them one can possibly investigate instanton/sphaleron processes of larger masses  $M_{\text{sph}}$  at hadron colliders.

Historically, the issue of instanton-induced decays was first noticed by Bjorken [33]. He pointed out that  $\eta_c$  decays have 3 large 3-body modes, several percents each of the total width:

$$\eta_c \rightarrow KK\pi; \pi\pi\eta; \pi\pi\eta'$$

Note that there is no  $\pi\pi\pi$  decay mode, or other decay modes we may think of without strangeness: the 't Hooft vertex *must* have all light quark flavors in it, including  $\bar{s}s$ .

More generally, charmonium decays are especially nice since one can use the well known  $J/\psi$  decays as a "control group", since its three-gluon annihilation mode does not go to operators that couple naturally to instantons. Indeed, the branchings of the 2- and 3-body decays of  $J/\psi$  are much smaller, and the average multiplicity of its decays is much larger than 3. That is why the few-percent branching of these 3-meson  $\eta_c$  decays is remarkable by itself.

The actual calculations of  $\pi\pi, KK, \eta\eta$  decays of scalar and  $KK\pi, \eta\pi\pi, \eta'\pi\pi$  decays of  $\eta_c$  were made by Zetocha and Schafer [34]. Their results contain rather high power of the instanton radius and therefore strongly depend on its value. So the authors used the inverted logic, evaluating from each data point the

<sup>5</sup>We are not aware of any study of  $\eta_b$  decays in this respect.

corresponding value of the mean instanton size  $\bar{\rho}$ . The results reproduced the decay widths reasonably well. Furthermore, these calculations provided about the most accurate evaluation of the average instanton size available, in the range of  $\bar{\rho} = 0.29 - 0.30 fm$ , common to all decay channels.

Let us start with the flavor composition. The specific form of the effective operator between light quarks induced by instantons has been derived by 't Hooft

$$(\bar{u}_R u_L)(\bar{d}_R d_L)(\bar{s}_R s_L) + (L \leftrightarrow R)$$

with the coefficients following from the LSZ reduction of the zero modes. For the the lightest quark clusters, of mass  $M \sim 3 GeV$ , we expect the production of 6 quarks in combination  $uuddss$ . Before discussing the decay modes, we need to look closer at  $N_f = 3$ .

## 6.2. The simplified forms of the effective Lagrangian

One issue is that in [34] the emitted mesons are treated in the “local approximation”, with the vertex Lagrangian directly projected to meson “decay constants” (which are the values of the wave functions at the origin). In reality, mesons fly with a momentum of about 1 GeV, for which the projections from the initial quasi-local state to the final state (the form factors) are not exactly one. This issue of “projection” (which we have already addressed above) gets more important as one considers sphalerons with larger masses.

Another (more technical) issue is the correct inclusion of all diagrams. Whatever form chosen for the 6-q Lagrangian, there are  $3! = 6$  channels (various connections of quarks and antiquarks), and they all needs to be included. While it is possible to go from one form to to another with Fierz transformation of operators, we were not sure all 6 connections were included on equal footing, and decided to repeat the calculation.

Another reason for redoing it is that the 3-flavor version of the Lagrangian used in [34] (their (26)) is very complicated, containing expressions with three color matrices and structure constants of the  $SU(3)$  group

$$f^{abc} \lambda^a \lambda^b \lambda^c, \quad d^{abc} \lambda^a \lambda^b \lambda^c$$

As we will show, these can be eliminated in favor of a simpler form, which we use. (In Appendix B.1 we will also show one more generic form of this Lagrangian based on the so called Weingarten coefficients of the product of unitary matrices averaged over the groups.)

We start by explaining the two main technical complications in this problem. A single instanton (or sphaleron) is constructed in a color  $SU(2)$  setting, with the gauge fields  $A_\mu^a T_{ij}^a$  with color indices  $i, j = 1, 2$ . The quark zero modes  $\psi_\alpha^j$  in the chiral representation ( $\gamma_5$  is diagonal) carry a matching spin index  $\alpha = 1, 2$  and color index  $j = 1, 2$ , coupled to each other in a “hedgehog” way.

However, the gauge group in QCD is  $SU(3)$  and in it, the instanton appears rotated from its standard form (just described) to some arbitrary 2d plane  $\in SU(3)$  by a unitary  $3 \times 3$  matrix, e.g.  $\psi_\alpha^a \rightarrow U_i^a \psi_\alpha^i$ . The 't Hooft effective Lagrangian contains  $2N_f = 6$  (or 8 or 10) quark zero modes, and therefore the 6-th (or 8-th or 10-th) power of this matrix. Although the explicit expressions for “isotropic” averaging of these powers of  $U$  have been known for some time (see e.g. appendix of [35]) these formulae are rather complicated, and contain convolutions with the structure constants  $f^{abc}, d^{abc}$  of  $SU(3)$ . Schafer and Zetocha [34] used such form, see eqn(26) of their paper.

Another technical issue is as follows. Multifermion operators can be identically represented in many different forms, since one can color-couple different  $\bar{q}q$  pairs. (Or even  $qq$  pairs as is convenient for color superconductivity and baryon production.) Those “Fierzing” transformations are jus identities, but with flavor, color and Dirac indices involved, they can create a multitude of operators. Yet, whatever form of the vertex operator is used, one still need to include it in all possible channels. For example, for the operator structure  $\bar{q}\bar{q}q\bar{q}q$  projected onto 3 mesons, there are obviously  $3! = 6$  ways to relate it to three mesonic  $\bar{q}q$  wave functions. For 8-q operators there are  $4!$ , etc.

Here and in Appendix Appendix B we show how one can simplify the operator structure, by keeping its flavor determinantal form intact, which has no structure constants as quoted in [36], and used for heavy-light

multi-quark systems [37]. We then explicitly do all possible convolutions with all mesonic wave functions in Mathematica, avoiding Fierzing altogether. More specifically [36] (See eq. 2.56)

$$\begin{aligned} \mathcal{V}_{qqq}^{L+R} = & \frac{\kappa}{N_c(N_c^2 - 1)} \left( \frac{2N_c + 1}{2(N_c + 2)} \det(UDS) \right. \\ & \left. + \frac{1}{8(N_c + 1)} \left( \det(U_{\mu\nu}D_{\mu\nu}S) + \det(U_{\mu\nu}DS_{\mu\nu}) + \det(UD_{\mu\nu}S_{\mu\nu}) \right) \right) + (L \leftrightarrow R) \end{aligned} \quad (23)$$

with a strength

$$\kappa = \frac{n_{I+\bar{I}}}{2} \left( \frac{4\pi^2 \rho^3}{M\rho} \right)^3 \quad (24)$$

and the short hand notations ( $Q \equiv U, D, S$ )

$$Q = \bar{q}_R q_L \quad Q_{\mu\nu} = \bar{q}_R \sigma_{\mu\nu} q_L \quad Q^a = \bar{q}_R \sigma^a q_L \quad (25)$$

with  $\sigma_{\mu\nu} = \frac{1}{2}[\gamma_\mu, \gamma_\nu]$ . Note that the spin contribution is sizably suppressed by  $1/8N_c$  in the large  $N_c$  limit, when compared to the scalar contribution. It is clear from our Fierzing arguments in Appendix Appendix B and symmetry, that only two determinantal invariants will survive after Fierzing as in (23), with only the structures  $UDS$  and  $U_{\mu\nu}D_{\mu\nu}S$  and their permutations allowed. The only non-trivial results are their weight coefficients. This observation holds for 4, 8 and 10 quark vertices as well, assuming they allow for zero modes. For instance, for 4-quark vertices the general structure is

$$\mathcal{V}_{qq}^{L+R} = \kappa_2 A_{2N} \left( \det(UD) + B_{2N} \det(U_{\mu\nu}D_{\mu\nu}) \right) + (L \leftrightarrow R) \quad (26)$$

which is readily checked to hold with

$$A_{2N} = \frac{(2N_c - 1)}{2N_c(N_c^2 - 1)} \quad B_{2N} = \frac{1}{4(2N_c - 1)} \quad (27)$$

Note that at large  $N_c$ , the suppression of the spin contribution is still exactly  $1/8N_c$ , with  $A_{\#q} \approx 1/N_c^\#$ . Remarkably, both the value of the  $A, B$  coefficients and their determinantal structures are fixed uniquely in this limit by symmetry and scaling. For completeness, the 8-quark vertices are of the form

$$\begin{aligned} \mathcal{V}_{qqqq}^{L+R} = & \kappa_4 A_{4N} \left( \det(UDSC) + B_{4N} \left( \det(U_{\mu\nu}D_{\mu\nu}SC) + \text{perm.} \right) \right. \\ & \left. + C_{4N} \left( \det(U_{\mu\nu}D_{\mu\nu}S_{\alpha\beta}C_{\alpha\beta}) + \text{perm.} \right) \right) + (L \leftrightarrow R) \end{aligned} \quad (28)$$

although for the heavy charm the use of the  $L, R$  zero modes may not be justified.

In the Weyl basis  $\sigma_{\mu\nu} \rightarrow i\eta_{\mu\nu}^a \sigma^a$  with the 't Hooft symbol satisfying  $\eta_{\mu\nu}^a \eta_{\mu\nu}^b = 4\delta^{ab}$ , and (23) can be simplified

$$\begin{aligned} \mathcal{V}_{qqq}^{L+R} = & \frac{\kappa}{N_c(N_c^2 - 1)} \left( \frac{2N_c + 1}{2(N_c + 2)} \det(UDS) \right. \\ & \left. - \frac{1}{2(N_c + 1)} \left( \det(U^a D^a S) + \det(U^a D S^a) + \det(UD^a S^a) \right) \right) + (L \leftrightarrow R) \end{aligned} \quad (29)$$

$\mathcal{V}_{qqq}$  is only active in flavor singlet 6-quark states. The flavor determinantal interactions can be made more explicit by using the permutation operators in flavor space as the symmetric group  $S_3$  of permutations is composed of  $3!$  terms only, 3 cyclic-permutations with positive signature and 3 pair-permutations with negative signature. Clearly, the 3-body instanton induced interaction (29) does not vanish only in flavor singlet  $uds$  states (repulsive). Its 2-body reduction is attractive in states with a pair of antisymmetric flavor diquarks  $ud$ ,  $us$ ,  $ds$  (attractive). A more explicit writing of (29) suitable for numerical analysis in terms of explicit  $3 \times 3$  flavor determinants is

$$\begin{aligned} \mathcal{V}_{qqq}^{L+R} = & \frac{\kappa}{N_c(N_c^2 - 1)} \left[ \left( \frac{2N_c + 1}{2(N_c + 2)} \right) \begin{vmatrix} \bar{u}_R u_L & \bar{u}_R d_L & \bar{u}_R s_L \\ \bar{d}_R u_L & \bar{d}_R d_L & \bar{d}_R s_L \\ \bar{s}_R u_L & \bar{s}_R d_L & \bar{s}_R s_L \end{vmatrix} \right. \\ & \left. - \frac{1}{2(N_c + 1)} \sum_{a=1}^3 \left( \begin{vmatrix} \bar{u}_R \sigma^a u_L & \bar{u}_R \sigma^a d_L & \bar{u}_R s_L \\ \bar{d}_R \sigma^a u_L & \bar{d}_R \sigma^a d_L & \bar{d}_R s_L \\ \bar{s}_R u_L & \bar{s}_R d_L & \bar{s}_R s_L \end{vmatrix} + \begin{vmatrix} \bar{u}_R \sigma^a u_L & \bar{u}_R d_L & \bar{u}_R \sigma^a s_L \\ \bar{d}_R u_L & \bar{d}_R d_L & \bar{d}_R s_L \\ \bar{s}_R \sigma^a u_L & \bar{s}_R d_L & \bar{s}_R \sigma^a s_L \end{vmatrix} + \begin{vmatrix} \bar{u}_R u_L & \bar{u}_R d_L & \bar{u}_R s_L \\ \bar{d}_R u_L & \bar{d}_R \sigma^a d_L & \bar{d}_R \sigma^a s_L \\ \bar{s}_R u_L & \bar{s}_R \sigma^a d_L & \bar{s}_R \sigma^a s_L \end{vmatrix} \right) \right] \\ & + (L \leftrightarrow R) \end{aligned} \quad (30)$$

### 6.3. Mesonic decays of sphalerons

Convoluting the vertex function in the form (30) with various mesons wave functions in all possible  $3! = 6$  ways we obtain the matrix elements for a number of 3-meson decay channels, listed in the Table. The meson definitions and couplings are defined in Appendix A.

|                 |                     | PDG2020                | input [34]            | —M—                         |
|-----------------|---------------------|------------------------|-----------------------|-----------------------------|
| $K\bar{K}\pi$   | $K^+K^-\pi^0$       | $7.3 \pm 0.4$ (all 4)  | $5.5 \pm 1.7$ (all 4) | $5.07 K_K^2 K_\pi$          |
|                 | $K^+\bar{K}^0\pi^-$ |                        |                       | $7.27 K_K^2 K_\pi$          |
|                 | $K^0\bar{K}^0\pi^0$ |                        |                       | $5.07 K_K^2 K_\pi$          |
|                 | $K^-K^0\pi^+$       |                        |                       | $7.27 K_K^2 K_\pi$          |
| $\pi\pi\eta$    | $\pi^+\pi^-\eta$    | $1.7 \pm 0.5$          | $4.9 \pm 1.8$ (both)  | $4.92 K_\pi^2 K_\eta^s$     |
|                 | $\pi^0\pi^0\eta$    |                        |                       | $2.46 K_\pi^2 K_{\eta'}^s$  |
| $\pi\pi\eta'$   | $\pi^+\pi^-\eta'$   | $4.1 \pm 1.7$ (both)   | $4.1 \pm 1.7$ (both)  | $5.20 K_\pi^2 K_{\eta'}^s$  |
|                 | $\pi^0\pi^0\eta$    |                        |                       | $2.60 K_\pi^2 K_{\eta'}^s$  |
| $\bar{K}K\eta$  | $K^+K^-\eta$        | $1.36 \pm 0.15$ (both) |                       | $3.68 K_K^2 F_\eta^q$       |
|                 | $K^0\bar{K}^0\eta$  |                        |                       | $3.68 K_K^2 F_\eta^q$       |
| $\bar{K}K\eta'$ | $K^+K^-\eta'$       |                        |                       | $3.53 K_K^2 F_{\eta'}^q$    |
|                 | $K^0\bar{K}^0\eta'$ |                        |                       | $3.53 K_K^2 F_{\eta'}^q$    |
| $\eta\eta\eta$  |                     |                        |                       | $1.32(K_\eta^q)^2 K_\eta^s$ |

Table 1: The first column gives the generic names of the decay channels of  $\eta_c$ , while the second column records the specific channels. The third column contains the corresponding branching ratio (percents) according to the Particle Data Table 2020. For comparison, we show in the fourth column the corresponding numbers used in [34]. The last column gives the decay matrix elements. The meson-specific constants (wave function at the origin) are defined in Appendix A.

Our first comment on the table is that in that two decades from the work in [34], some of the experimental branching ratios have improved their accuracy, while some are substantially modified. This needs to be kept in mind when comparing the predictions to experiment.

Of course, we can construct many ratios out of the Table. Here, we will mention two in particular

$$\begin{aligned} \frac{\Gamma(K\bar{K}\pi)}{\Gamma(\eta\pi\pi)} &= \frac{\sum |M|^2 0.111}{\sum |M|^2 0.135} \approx 10 \quad \left( \text{exp} : \frac{7.3 \pm 0.4}{2.55 \pm 0.75} \right) \\ \frac{\Gamma(\eta\pi\pi)}{\Gamma(\eta'\pi\pi)} &= \frac{\sum |M|^2 0.135}{\sum |M|^2 0.0893} \approx 0.9 \quad \left( \text{exp} : \frac{2.55 \pm 0.75}{4.1 \pm 1.7} \right) \end{aligned} \quad (31)$$

where the last ratio corresponds to the three-body phase space. The ratios are only in qualitative agreement with the reported measurements. Clearly more studies are needed.

#### 6.4. Baryonic decays of sphalerons

Another fascinating issue, not so far discussed in the literature, is whether the 6-fermion effective Lagrangian can be used to produce a *baryon-antibaryon* pair, rather than 3 mesons.

At first sight one finds a problem which looks quite severe. The operator involves the quark set  $u, d, s$ , and the natural baryons to look at are  $\Lambda$  or  $\Sigma^0$  baryons. As for any baryon, their color wave function is antisymmetric in color,  $\epsilon_{c_1 c_2 c_3}$ . The flavor determinant is also antisymmetric in flavor  $\epsilon_{f_1 f_2 f_3}$ . Fermi statistics then require the remaining part of the wave function to be antisymmetric. In the lowest shell of the quark model, this remaining part is made of three quark spins. It is not possible to create  $\epsilon_{s_1 s_2 s_3}$  spin wave functions, since the spin indices are 1, 2 only. Indeed it is well known, that the lowest baryonic octet does not have the ninth state, a singlet, unlike the mesons.

This notwithstanding, let us also approach the issue phenomenologically. we assume, following Bjorken, that  $\eta_c$  decays possess topological paths, while  $J/\psi$  decays do not. So, what do we see in the baryonic sector?

Both  $\eta_c$  and  $J/\psi$  have observed decays into  $\bar{\Lambda}\Lambda$ , with similar branching  $\sim 10^{-3}$ . Yet their absolute widths differ by roughly a factor of 200, in favor of the former case. What speaks against the topological mechanism is the fact that in both cases the channels  $\bar{p}p$  and  $\Sigma^+\Sigma^-$  have similar yields to  $\bar{\Lambda}\Lambda$ , although they cannot follow from our 6-fermion effective vertex.

In summary, topological production of  $\bar{\Lambda}\Lambda$  does not appear to take place in  $\eta_c$  decays.

Yet, if the sphaleron mass is larger than 3 GeV, one may think of production of two higher mass baryon resonances. Among those there are known  $SU(3)$  singlets, which are anti-symmetric in flavor. The lowest of them are

$$\Lambda(1405) : J^P = 1/2^-, \quad \Lambda(1520) : J^P = 3/2^-$$

Their negative parity is explained in the quark model by a unit of orbital momentum  $L = 1$ . Unfortunately, this negative parity also protect them from any mixing with the usual  $\Lambda$ . As they are well known resonances, their back-to-back production should be quite noticeable. Their widths are  $\Gamma = 50$  and 157 MeV, respectively. They both have very characteristic decays,

$$\Lambda(1405) \rightarrow \Lambda\gamma, \quad \Lambda(1520) \rightarrow \Sigma\pi$$

with branching ratios of the order of 50% for both.

#### 6.5. Chirality correlation in baryonic decays

The  $\bar{\Lambda}\Lambda$  channel is the most interesting for two reasons:

(i) Zero isospin means that  $(ud)$  diquark has spin zero, and therefore the whole spin of  $\Lambda$  is carried by its strange quark;

(ii) weak decays of  $\Lambda$  hyperon allows to observe its polarization. Indeed, in the decay  $\Lambda \rightarrow p\pi^-$  of polarized hyperon, the direction of the proton is mostly along the initial polarization direction.

As a measure of  $s$  quark chirality one can use

$$\xi_\Lambda \equiv \cos(\theta(\vec{p}_\Lambda \vec{p}_p)) \tag{32}$$

and calculate the distributions  $P(\chi_{\Lambda\bar{\Lambda}})$  over the *relative chiralities*, the product of

$$\chi_{\Lambda\bar{\Lambda}} \equiv \xi_\Lambda \times \xi_{\bar{\Lambda}} \tag{33}$$

Ordinary perturbative diagrams with one or two gluons (or photons) leading to the production of a strange quark pair are “vector-like”, meaning that the chiralities are the same,

$$(\bar{s}_L s_L) + (\bar{s}_R s_R)$$

This means either both  $\xi$  are positive, or both negative, leading to  $\chi_{\Lambda\bar{\Lambda}}$  positive.

On the other hand, the instanton/sphaleron-induced vertex is, *non – diagonal* in chirality

$$(\bar{s}_L s_R) + (\bar{s}_R s_L)$$

The produced  $\Lambda$  and  $\bar{\Lambda}$  should therefore have the *opposite* chiralities, and  $\chi_{\Lambda\bar{\Lambda}}$  is negative. We are not aware of such study even in any inclusive reactions, in which a pair of Lambda hyperon decays are identified with some reasonable statistics.

As we discussed above, the exclusive production of  $\bar{\Lambda}\Lambda$  from the t' Hooft-like Lagrangian is not possible. Yet strong chirality correlations in question would perhaps persist in channels with other associate hadrons. For example, in the production of  $\bar{\Lambda}(1405)\Lambda(1405)$  with their subsequent radiative decays into  $\Lambda + \gamma$ , there should remain rather significant correlation of polarizations.

If observed, it would be an excellent indication of the topological origin of the vertex, pointing to an explicit violation of the  $U_A(1)$  symmetry.

## 7. Sphaleron decays at medium masses:

### $M = 10 - 20$ GeV and 10-fermion operators

#### 7.1. Charm pairs and decays with 8-fermion operators

The field magnitude at the center of the instantons is comparable to  $m_c^2$ . Although charm is not usually treated as a light flavor, it must have a certain coupling to instantons. The fact of large instanton-induced decays of  $\eta_c$  confirms this idea.

The 8-flavor operators have also a flavor-asymmetric structure

$$V \sim (\bar{u}u)(\bar{d}d)(\bar{s}s)(\bar{c}c)$$

with a typical determinantal structure. There are  $4! = 24$  4-meson channels one should think of: for example those can be the same 3-meson channels discussed above,  $\pi\pi\eta, \pi\pi\eta', KK\pi$  with an *added*  $\eta_c$ . The other quite distinct channels are e.g.  $KKDD$  *without* any pions. Note also that 4 pseudoscalar mesons without orbital momentum correspond to operator  $G^2$ , not the pseudoscalar one.

#### 7.2. Multi-gluon production

We already mentioned several times, that the total sphaleron mass is  $\mathcal{O}(3\pi^2/g^2\rho)$  while the energy of produced gluons are only  $\mathcal{O}(1/\rho)$ . The gauge quanta multiplicity is therefore  $\sim 1/g^2 \sim \mathcal{O}(100)$  in the electroweak theory and  $\mathcal{O}(10)$  in QCD.

Therefore, in the “medium sphaleron mass” range indicated, the energy per gluon is in the range  $E_g = 1 - 2$  GeV. We know, from lattice studies and models, that under such conditions gluons are not yet “partons” with independent life. Instead, they are paired into the lowest glueball states with masses

$$M_{0+} \approx 1.6 \text{ GeV} \quad M_{2+} \approx 2.2 \text{ GeV} \quad (34)$$

So, we propose that in this mass range a significant part of the energy will go into several lowest glueballs. All of them are now reasonably well identified with scalar and tensor resonances.

#### 7.3. Semiclassical production in constant electric field and in sphaleron explosion

Another new interesting option is the production of  $\bar{b}b$  pair by sphaleron decays.

Before we provide some estimates, let us recall how the related classic problem *of the pair production of  $e^+e^-$  in a constant electric field* can be described semiclassically. It is widely known as the Schwinger process, as he solved it in detail in 1950. However, we will discuss neither the Schwinger paper, nor even the earlier Heisenberg-Euler paper, but the much earlier semiclassical work [38] from 1931 (well before anyone else).



The EOM of a charge relativistically moving in constant electric field is a classic problem which everybody had encounter in E/M classes. Writing it in the usual Minkowski form

$$\frac{dp}{dt} = \frac{d}{dt} \left( \frac{v}{\sqrt{1-v^2}} \right) = \frac{eE}{m} \equiv a \quad (35)$$

yields the hyperbolic solution

$$v_M(t) = \frac{at}{\sqrt{1+a^2t^2}}, \quad x_M(t) = \frac{1}{a} (\sqrt{1+a^2t^2} - 1) \quad (36)$$

for a particle that starts at rest with a nonrelativistic acceleration,  $x_m = at^2/2$ . At large times, the motion turns ultrarelativistic with  $v_M \rightarrow 1$ .

The analytical continuation of the the trajectory to Euclidean time  $\tau = it$  yields

$$v_E = \frac{a\tau}{\sqrt{1-a^2\tau^2}}, \quad x_E(\tau) = \frac{1}{a} (\sqrt{1+a^2\tau^2} - 1) \quad (37)$$

At time  $\tau = 0$  the particle is at the origin with zero velocity,  $x_E = 0, v_E = 0$ . For  $-1/a < \tau < 1/a$  it describes an Euclidean path in shape of a semicircle. In Euclidean space, the world-time is no different from the other coordinates, and the electric field  $G_{01}$  is not different from the magnetic field, so in the 0-1 plane the paths are circles, like they are in all other planes.

To understand the physical meaning of the semicircle (blue dashed line) in the Dirac sea interpretation one needs to split it into two halves. The path describes tunneling through the “mass gap”, between energies  $-M$  and  $M$  in the spectrum of states. In Minkowski space there are no states between  $E = -\sqrt{p^2 + m^2}$  and  $E = \sqrt{p^2 + m^2}$  with real momentum  $p$ , In the Euclidean world however, the momentum is imaginary!

Let us note that the rapidity  $y_M = \text{arctanh}(v_M)$  in Minkowski space, becomes in Euclidean space a rotation angle

$$y_E = \arctan(v_E) = \arctan\left(\frac{a\tau}{\sqrt{1-a^2\tau^2}}\right) \quad (38)$$

and at  $\tau = \pm 1/a$  it is  $\pm\pi/2$ . The action  $S = \int(-m ds - eE x dt)$  when evaluated with the Euclidean path gives  $S_E = \pi m^2/2eE$ . The semiclassical probability (square of the amplitude) of the pair production is then

$$P \sim e^{-2S_E} \sim e^{-\pi m^2/eE} \quad (39)$$

When discussing the heavy quark production we will assume that the back reaction of the produced quark on the gauge field can be neglected. This implies that the total sphaleron mass is much larger than that of the produced pair

$$\frac{3\pi^2}{g^2(\rho)\rho} \gg 2M \quad (40)$$

For  $\rho \sim 1/3 \text{ fm}$ , corresponding to the maximum in the instanton size distribution, the l.h.s. is about  $M_{\text{sph}} \approx 3 \text{ GeV}$ . Therefore, the condition is satisfied for the strange quark pair  $\bar{s}s$  but not for the charm quark pair  $\bar{c}c$ .

The electric field during the sphaleron explosion  $E_a^m(\vec{x}, t)$  follows from the expressions for the field potential (16). The component with  $a = 3$  corresponds to the diagonal Pauli generator  $\tau^3$ , so that quark color remains unchanged. The maximal magnitude of the field corresponds to the  $x^3$  or  $z$  direction,  $E_3^3$ . The formula is a bit long to give here, but its behavior is shown in Fig. 6

From our discussion of the semiclassical quark pair production in a *homogeneous* electric field it follows that the field must produce an impulsions

$$\Delta p = \int E dt \sim M$$

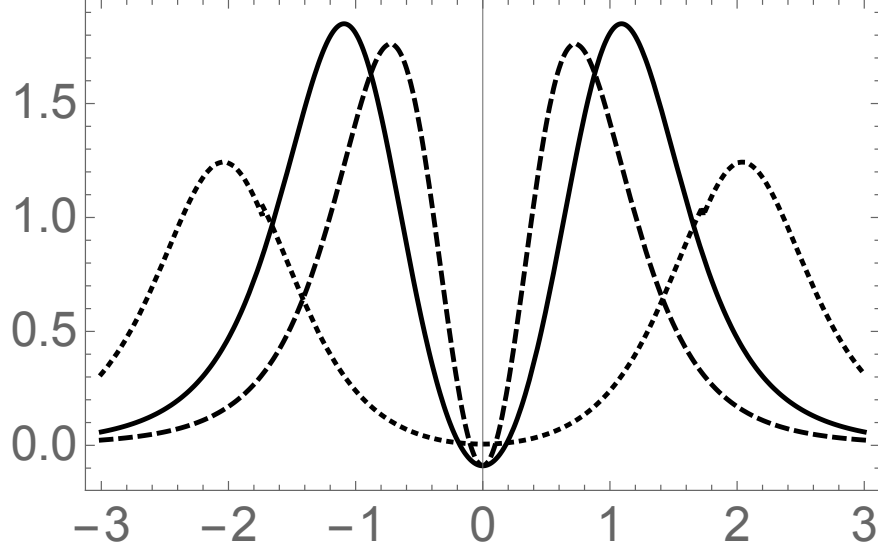


Figure 6: The snapshots of the electric field component  $E_3^3(r, t)$  in units of  $1/g\rho^2$ , as a function of  $x^3/\rho$ , for times  $t/\rho = 0.5$  (dashed),  $t/\rho = 1$  (solid) and  $t/\rho = 2$  (dotted) curves.

to reach, in Euclidean notations, the rotation angle  $y_E = \pi/2$  needed to make it real. For an estimate, one can take  $E \approx 1.5/\rho^2$  and  $\delta t \approx \rho$  ( following Fig. 6), from which the estimated impulsion is

$$\Delta p = E\delta t \approx 1.5/\rho$$

This gives an estimated limit for the mass  $M$  of a quark which is *likely* to be produced

$$M < 1.5/\rho \tag{41}$$

Using  $1/\rho = 0.6 \text{ GeV}$ , one finds the r.h.s. to be  $\approx 1 \text{ GeV}$ . This implies that strange quarks, with  $M_s \sim 0.14 \text{ GeV}$  can be produced, but not the charmed ones, with  $M_c \sim 1.5 \text{ GeV}$ . To satisfy this estimate, one would need to decrease  $\rho$  by about a factor 2. To produce a  $b$  quark, with  $M_b \approx 5 \text{ GeV}$ , one would need to decrease  $\rho$  by a factor 6 or so.

In order to get quantitative semiclassical description one has to do the following: (i) convert the expressions for the field to Euclidean time; and (ii) solve the relativistic classical EOM

$$M \frac{du^\mu}{ds} = F^{\mu\nu} u_\nu$$

where  $u^\mu = dx^\mu/ds$  and  $s$  is the proper time,  $ds^2 = dt^2 - d\vec{x}^2$ . Comparable and rather complex electric and magnetic fields make the paths quite complicated. On top of that, the result depends on the starting location of the particle. So, at this time, we have no results on such a calculation to report.

## 8. Sphaleron decays at large masses, $M \sim 100 \text{ GeV}$

These masses fall in the range discussed in the theoretical literature, and mostly searched at HERA and LHC, as they promise to have  $\mathcal{O}(10)$  well recognized gluonic and quark jets. Background evaluation for such events were attempted, using current event generators tuned to multi-jet events.

Two comments are in order:

(i) In this mass range, it is possible to use double diffractive events at LHC, which are expected to reduce backgrounds substantially in comparison to ambient  $pp$  collisions.

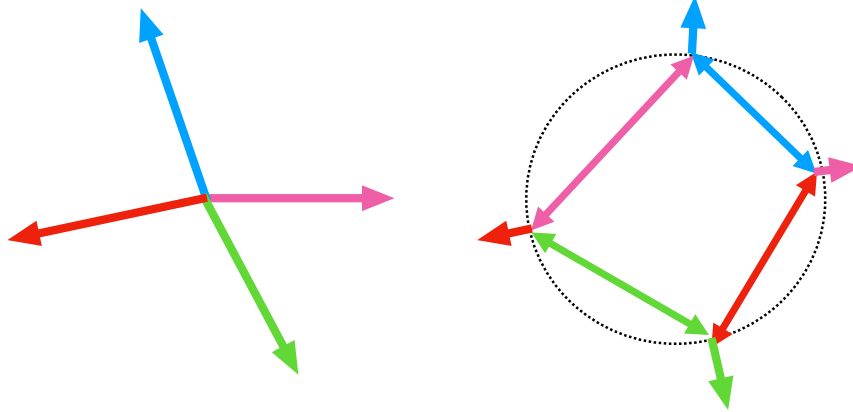


Figure 7: Schematic picture illustrating the configuration of QCD strings in four-jet events. The left corresponds to the usual case, when jets originate from collisions at the origin in the transverse plane. The right corresponds to an exploding sphaleron in which the strings are not connected to the origin, but are close to the expanding shell (dotted circle).

(ii) In the usual parton-parton collisions, the fragmentation function of  $\mathcal{O}(10 \text{ GeV})$  gluons is essentially the product of string breaking. One end of these strings is on the leading gluon, the other ends at throughgoing partons, or the origin in the transverse plane, see Fig. 7 left. But sphaleron decay leaves out the interior of the exploding shell “empty” (more precisely, with a pure gauge configuration). As these gluons become physical and separated from each other, the strings would go *between* them close to the shell, rather than extending to the origin, see Fig. 7 right. This suggests the appearance of some unusual gluon jet fragmentation functions, with a significant depletion at small  $p_t$ .

## 9. Magnetic field and Chiral Magnetic Effect

In the presence of an electromagnetic field  $\vec{b}_{EM}$  and chiral disbalance of fermions, there exists the so called Chiral Magnetic Effect (CME), an electric current along  $\vec{b}_{EM}$  is created, for a review see [39]. Experiments aimed at observing it in heavy ion collisions at RHIC have been made, lately utilizing beams of nuclei with the same atomic weight but different charges, but the analysis is not conclusive. The CME was observed in semi-metals [39].

An interesting manifestation of the phenomenon must also be present in the instanton-sphaleron production processes, which we propose in this paper.

The first part of it, related with instantons, has already been studied. While calculating nucleon form factors using instantons [40], Faccioli observed that the instanton zero mode acquires an electric dipole along the magnetic field. (Of course, adding the antiinstanton contribution cancels it, unless the topological  $\theta$  angle is nonzero). Lattice simulations in a magnetic field carried in [41] have confirmed reality of this effect.

The extensive analytic study of the electric dipole moment of a zero mode is due to Basar, Dunne and Kharzeev [42]. Let us just recall a qualitative explanation of the mechanism from their work. The Dirac equation in the instanton background conserves total

$$\vec{J} = \vec{L} + \vec{S} + \vec{T}$$

the sum of orbital momentum, spin and (SU(2)) isospin. As noticed by t’Hooft, the isospin-orbit ( $\vec{T} \cdot \vec{L}$ ) term forces orbital momentum *not* to be a good quantum number. Therefore, it is possible to mix opposite parity states<sup>6</sup>. The external electromagnetic field  $\vec{b}$  couples spin to angular momentum, and induces such

<sup>6</sup>This discussion is in the instanton background, which is CP non-invariant. The QCD vacuum and other states are CP conserving.

mixing. The zero fermion and antifermion modes are deformed in different directions, creating a nonzero electric dipole along the  $\vec{b}$  field. (Antiinstantons of course would do the opposite: we discuss local, not global CP violation.) No observable consequences of this effect have so far (to our knowledge) been proposed.

Now, consider e.g. very peripheral heavy ion collisions, in which Pomeron-Pomeron (or  $\gamma$ -Pomeron or  $\gamma\gamma$ ) collision initiate instanton-sphaleron production process. As usual, the large electric charges of the ions generate a strong magnetic field at the production point. The exploding instanton and sphaleron gauge field remains spherical, but, since the quark zero mode is deformed, the exploding electric field will carry them differently in direction of the magnetic field, as compared to two other directions, producing anisotropy of the quark momenta.

The effect of a magnetic field can be seen by comparing  $pp$  and  $PbPb$  peripheral collisions. The orientation of the collision plane (to which  $\vec{b}$  is normal) can be deduced from the direction of two forward-moving protons (or ion remnants).

The sign of the effect for a quark depends on its electric charge, and the light quarks in question,  $u, d, s$  have charges  $+2/3, -1/3, -1/3$ . So, for the mesons  $\pi^+$  versus  $\pi^-$  (kaons, etc) the effects are added, resulting in a charge-dependent deformation of the distribution. The instanton and antiinstanton events still produce opposite signs of the effect. So one may construct a meson *correlation* observable inside an event (*all*  $\pi^+$  have one preferred direction, opposite to  $\pi^-$ ).

Another (statistically challenging) option is to select events with  $\Lambda$  (or  $\bar{\Lambda}$ ) decays, which tells us about the strange quark chirality. Statistically selecting “more-likely-instanton” or “more-likely-antiinstanton” events, one can perhaps see an electric dipole in the event directly.

Concluding this discussion, let us again emphasize the following. The instanton-sphaleron process is the “hydrogen atom” of topological effects. The chiral correlations produced in it is maximally possible, as all quarks and antiquarks have fixed chiralities. (For comparison, in heavy ion collisions we think the axial charge of the fireball is between  $\pm 20$  or so, on top of thousands of unpolarized ones. While the proposed measurements may appear quite exotic, the cross sections are relatively large, allowing LHC with the right trigger to produce billions of diffractive events.

## 10. The “entrance factor”

So far our discussion was mostly semiclassical, we considered (Euclidean) tunneling paths and (Minkowski) sphaleron explosions. Then we projected the outgoing quanta to some final hadronic states.

Now we focus on the very initial stage of the collision. Here we first have to make hard choices, selecting theoretical tools for its description. Here are these choices: colliding protons can be seen as colliding (i) partons (gluons or quarks); (ii) color dipoles; (iii) glueballs; or (iv) Pomerons. Let us briefly discuss them subsequently.

At high mass scale, e.g. the sphaleron mass squared

$$s' = M_{\text{sph}}^2 \gg 100 \text{ GeV}^2$$

the parton-parton collision is the natural perturbative description, developed since the 1970’s in the context of jets or heavy quanta production. It was applied by Ringwald and Schrempf for DIS at HERA [43], and now by Khoze et al. [44] to LHC setting, incorporating Mueller perturbative correction [45]. For comparison of these predictions with HERA data see [46], and with LHC [47]. At high mass regime the theoretical predictions have reasonable uncertainties, such as in the semiclassical prefactor, but the main difficulty in it is large background induced by ambient events. The main observable is a spherical multi-jet events.

To illustrate the situation, we show the gluon-gluon cross section  $\sigma(\sqrt{s'})$  of the instanton-sphaleron process in Fig.8. The points are from Table 1 by Khoze et al. [44]. The instanton size in the range of the plot changes from  $1/\rho = 1 \text{ GeV}$  to  $75 \text{ GeV}$ , and the number of outgoing gluons at the high end reaches about a dozen.

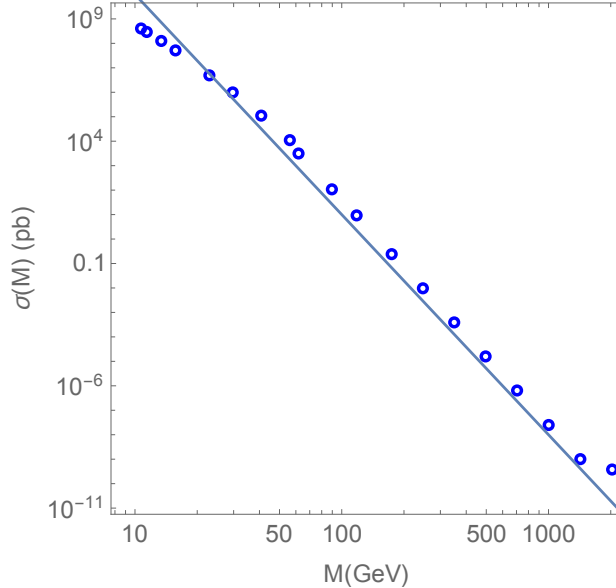


Figure 8: Cross section  $\sigma(M)$  in pb of the process gluon-gluon-instanton/sphaleron, versus the sphaleron mass  $M(\text{GeV})$ . The points are explained in the text, the line is the  $1/M^9$  background dependence shown for comparison.

The line, shown for comparison, is  $1/M^9$ . Recall that the one-loop coefficient of the QCD beta function is  $b = (11/3)N_c - (2/3)N_f$ , or 9 if the number of light flavors  $N_f = 3$ . The effective action is twice that of the instanton  $2S_{inst}$  minus its depletion for sphaleron production  $-\Delta S$ . The cross section should be, by dimension,

$$\sigma \sim \frac{1}{M^2} \left( \frac{\Lambda_{QCD}}{M} \right)^{b(2-\Delta S/S_0)}$$

One can see that the original estimates

$$\frac{\Delta S}{S_0} \approx 1 \quad (42)$$

are supported by actual multidimensional integration.

The calculation along a path including both the Euclidean and Minkowskian times has been performed in [48], in the electroweak setting. Their result (solid line in Fig.6 of that paper) shows that the action is reduced from  $\approx 12.5$  at the zero sphaleron mass to about  $\approx 7$  at the large sphaleron mass. It also supports the estimate (42).

The backgrounds come from multiple QCD reactions, which have cross sections

$$\sigma_{background} \sim \frac{\alpha_s^2}{M^2}$$

It is therefore clear that the task of separating the signal from the background becomes much harder as the cluster mass  $M$  grows.

As the momentum transfer scale decreases, one may naturally think of coherent contribution of two (or more) partons. Color neutrality can be implemented starting from color dipoles. Unlike partons, the colliding color dipoles have a natural scale given by their sizes  $a_1, a_2$ . Correlating dipoles with instantons via Wilson loops has been done by us [16]. The cross sections obtained can be directly tested in double-inelastic electron-positron (or  $\gamma^* \gamma^*$ ) collisions. Unfortunately, a description of a proton in terms of color dipoles is not yet (to our knowledge) developed.

At small momentum transfer scale – in diffractive processes we will focus on – the colliding objects are described in terms of (reggeized) hadron exchanges, especially by tensor glueballs or (their extension to the

whole Regge trajectory), the Pomerons. In a number of relatively recent works it has been shown that Pomeron exchanges require effective description in terms of symmetric tensor. These facts, together with overall development of holographic QCD models, had strengthen the Pomeron-graviton connection.

## 11. Sphaleron production in Pomeron-Pomeron collisions

We start with some general remarks related to experimental setting.

Double-Pomeron production processes at LHC are only at their initial stage. A general but brief discussion of the existing detectors was made in section 1.2. Let us only add that apparently in the standard high luminosity LHC runs, one cannot access masses less than say hundreds of GeV, but can go to any masses provided the dedicated low-luminosity runs are performed.

As we will detail below, Pomeron-Pomeron vertices are coupled to two operators, scalar  $G^2$  and pseudoscalar  $G\tilde{G}$ . The former is maximal when electric field directions are parallel, in the second orthogonal. Momentum kicks to two protons are directed with electric field. Therefore, locating roman pots in different azimuth, one can in principle “tag” and separate these two contributions.

Returning now to current experiments at LHC, we note that exclusive channel  $\pi^+\pi^-$  has been already studied by CMS [49], for invariant masses till  $M < 2$  GeV. It shows a  $\rho$ -meson peak, and contains hints at some other resonances.

Heavier clusters unfortunately were only studied by the old UA8 collaboration [3] with  $p\bar{p}$  collisions at the SPS. The production cross section in Pomeron-Pomeron collisions at the peak  $M \sim 3$  GeV is rather large  $\sigma_{PP} \sim 4$  mb.

But, as usual, what really matters is the Signal/Background (S/B) ratio. In this respect our only normalization process is the  $\eta_c$  decay. Assuming standard  $\bar{c}c \rightarrow gg$  annihilation, into  $G_{\mu\nu}\tilde{G}_{\mu\nu}$  pseudoscalar operator, one realizes that the gluon can either enter the instanton/sphaleron tunneling, or produce quark pairs perturbatively. Most likely, at fixed  $M_{gg}$  *it does not matter whether  $gg$  came from  $\bar{c}c$  annihilation or Pomeron-Pomeron collisions.*

In total, the three prominent 3-meson channels ascribed to the former have certain branching ratio, from which one can conclude that

$$\left(\frac{Signal}{Background}\right)(M \approx 3 \text{ GeV}) > 0.15$$

One can think of many other modes, e.g. with glueballs, scalar or pseudoscalar, but at a mass of only  $M_{\eta_c} \approx 3$  GeV those would be suppressed by phase space <sup>7</sup>. Perhaps it increases the signal by a factor of 2 or something like that. Alternatively, **PP** collisions can be approximated as  $gg + gg$  collisions, or operators with *two* stress tensors. This perhaps increases the background, say also by a factor of 2, so that these effects cancel out in the S/B ratio.

What is however even more important, if one looks in the “instanton-induced” channels there would hardly be any background. It follows from comparison of the  $\eta_c$  decays to  $KK\pi, \pi\pi\eta$  yields with pure pion final states.

Now, we address the sphaleron mass distribution in **PP** collisions. We already discussed in 5 the instanton size distribution

$$\frac{dn}{d\rho} \sim \left(\frac{1}{\rho^5}\right)(\rho\Lambda)^b \exp(-2\pi\sigma\rho^2) \quad (43)$$

with  $b = (11/3)N_c - (2/3)N_f$  is the first coefficient of the beta function, and  $\sigma \approx (0.42 \text{ GeV})^2$  the string tension. When combined with the (pure gauge) expression of the sphaleron mass  $M_{sph} = 3\pi^2/g^2\rho$ , it yields

---

<sup>7</sup>For a more accurate estimate, one needs to figure out which other modes come from the signal. Unfortunately there are many modes and their branching ratios are at the level less than a percent, so it would be hard if not impossible to get an accurate number.

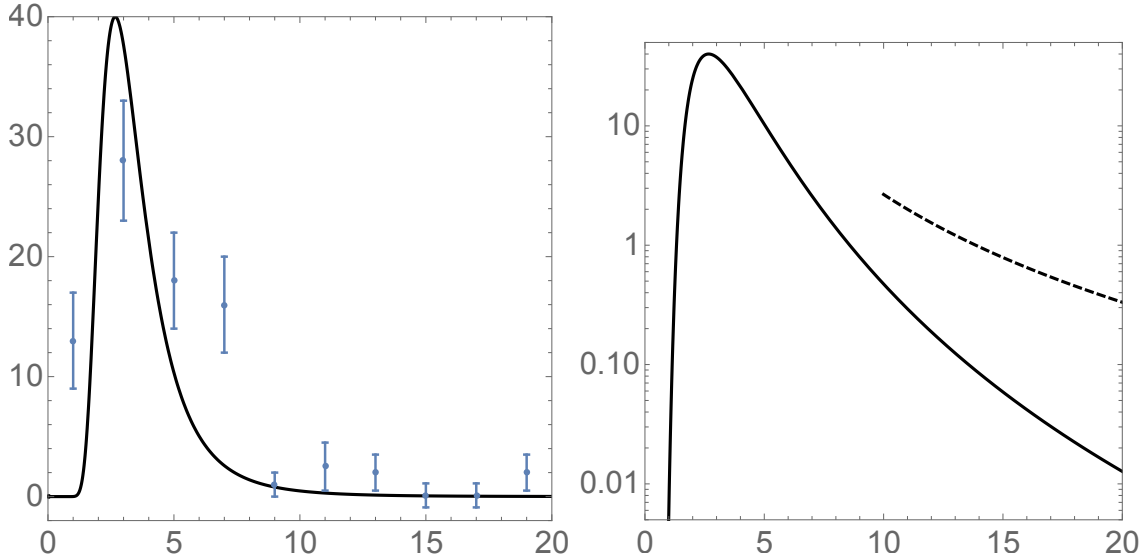


Figure 9: Left plot: Semiclassical distribution over the cluster mass  $M$  (GeV), compared to the data points from the UA8 experiment; Right plot is the logarithmic representation of the same curve (solid), now compared with the dashed line representing the perturbative background.

the distribution over this mass. In Fig. 9 we compare it with the data points from the UA8 experiment [3] (left plot), and with the background (right plot) expected to scale as  $d\sigma/dM \sim 1/M^3$  and normalized to the high-mass UA8 data.

As one can see, the vacuum distribution in instanton sizes and the experimental cluster mass distribution are in qualitative agreement in shape, and in predicted position of a peak. This supports our suggestion that those clusters may in fact be QCD sphalerons.

Let us make few other points:

- (i) the instanton-sphaleron production seems to be dominant at  $M \sim \text{few} - \text{GeV}$ ;
- (ii) the cross section to  $M \sim 20 \text{ GeV}$  decreases by about three orders of magnitude. With the efficiency of the forward trigger of UA8, about 1300 events were detected at *theSppS*. The luminosity of LHC is more than enough to cover these extra three orders of magnitude;
- (iii) where the signal-to-background ratio is about 1 : 20. The background – mostly two-jet events – is very anisotropic, so perhaps the identification of an isotropic signal can still be possible, even at  $M \sim 20 \text{ GeV}$ ;
- (iv) we recall that the clusters with  $M \sim 20 \text{ GeV}$  are the ones in which 10 quark operators (with pairs of  $\bar{b}b$  quarks) can be produced.

## 12. Sphaleron-gluon-quark vertex

To make explicit the sphaleron-quark vertex, we note that the instanton density in (24) follows from the averaging of the gluon field in the instanton vacuum

$$n_{I+\bar{I}} = n_I + n_{\bar{I}} = \frac{\alpha_s}{8\pi} \langle G^2 \rangle \quad n_{I-\bar{I}} = n_I - n_{\bar{I}} = \frac{\alpha_s}{8\pi} \langle G\tilde{G} \rangle \rightarrow 0 \quad (44)$$

where the second averaging is zero for  $\theta = 0$ . The normalizations in (44) are fixed by the QCD scale and axial anomalies in the instanton vacuum, respectively. Note that in (44)  $G^2$  and  $G\tilde{G}$  count the number of instantons and anti-instantons.

The single instanton-six-quark vertex and anti-instanton-six-quark vertex follow by omitting the vacuum averaging in (44), and recalling that the left-vertex is induced by an instanton, and the right vertex by an anti-instanton. More specifically, from (23) and (44) we obtain

$$\mathcal{L}_{Gqqq} = \left[ \frac{\alpha_s}{16\pi} \left( G^2 + G\tilde{G} \right) \right] \left( \frac{4\pi^2 \rho^3}{M\rho} \right)^3 \left[ \frac{\mathcal{V}_{qqq}^L}{\kappa} \right] + \left[ \frac{\alpha_s}{16\pi} \left( G^2 - G\tilde{G} \right) \right] \left( \frac{4\pi^2 \rho^3}{M\rho} \right)^3 \left[ \frac{\mathcal{V}_{qqq}^R}{\kappa} \right] \quad (45)$$

The sphaleron produced in the diffractive process is half a tunneling process with half the topological charge, and not self-dual. At the turning point, the sphaleron drags six quark zero modes out of the QCD vacuum with at  $t = 0$  the vertex mediated by  $G_S^2 = 2B^2$  since  $G\tilde{G}_S = 4E \cdot B = 0$

$$\begin{aligned} \mathcal{L}_{Sqqq}(t=0) = & \left( \left[ \frac{\alpha_s}{16\pi} G_S^2 \right] \left( \frac{4\pi^2 \rho^3}{M\rho} \right)^3 \left[ \frac{\mathcal{V}_{qqq}^L + \mathcal{V}_{qqq}^R}{\kappa} \right] \right)_{t=0} \\ & + \left( \left[ \frac{\alpha_s}{16\pi} \dot{K}_{0S} \right] \left( \frac{4\pi^2 \rho^3}{M\rho} \right)^3 \left[ \frac{\mathcal{V}_{qqq}^L - \mathcal{V}_{qqq}^R}{\kappa} \right] \right)_{t=0} \end{aligned} \quad (46)$$

and by the rate of the Chern-Simons charge density  $\dot{K}_{0S}$  following from  $\partial^\mu K_\mu = G\tilde{G}$ .

### 13. Witten amplitude for diffractive production $pp \rightarrow ppX$

QCD is difficult to track in the infrared since its fundamental quark and gluon constituents repackage in confined hadrons. The ensuing hadronic dynamics is strongly coupled. Holographic QCD is a proposal guided by the AdS/CFT or gauge/gravity duality discovered in string theory. The holographic duality or principle states that boundary operators in the gauge theory can be mapped to a higher dimensional string theory in bulk in a curved anti-deSitter space. The original correspondence holds for type IIB superstring theory in  $AdS_5 \times S_5$ , but is commonly assumed to hold for a string theory in a general background. The string theory is in general difficult to solve, but in the double limit of a large number of colors and strong gauge coupling  $\lambda = g^2 N_c$ , it reduces to a weakly coupled supergravity in the classical limit, with a weak string coupling  $g_s = g^2/4\pi$ . The gauge invariant operators at the boundary are mapped onto supergravity fields in bulk with pertinent anomalous dimensions.

The n-point functions at the boundary of  $AdS_5$  follow from variation of the on-shell supergravity action in bulk with respect to the boundary values. The results are tree-level Feynman graphs with fixed endpoints on the boundary also known as Witten diagrams. The Witten diagram for the diffractive process of interest in this work  $pp \rightarrow ppX$  is illustrated in Fig. 10. The insertions on the  $AdS_5$  boundary refer to 4 nucleon operator insertions  $\mathcal{O}_{pi=1,\dots,4}$  and a glueball insertion  $\mathcal{O}_{X=G^2, G\tilde{G}}$ .  $\mathcal{O}_p$  sources a Dirac fermion in bulk with anomalous dimension  $M = \tau - 3/2$  ( $\tau$  refers to the twist, with typically  $\tau = 3$  to reproduce the hard scattering rules), and the  $\mathcal{O}_X$  sources a dilaton or axion in bulk with anomalous dimension  $\Delta_X = 4$ . In the Regge kinematics, the exchange in bulk is mediated by two closed string producing a dilaton  $h$  or an axion  $a$  which is equivalent to Pomeron-Pomeron fusion into  $h, a$  ( $\mathbf{PP} \rightarrow h, a$ ).

The Holographic construction provides a first principle description of the Pomeron ( $\mathbf{P}$ ) as a dual to a close string exchange [50, 11] or Reggeized graviton in bulk [5, 6]. In this section we will use this framework to extract the differential cross section for the reaction  $pp \rightarrow ppX$  through  $\mathbf{PP}$  fusion as discussed in [7] for pseudoscalar emission, and in [51] for Higgs production. After a brief description for the pertinent kinematics for this process in the Reggeized limit, we will summarize the main formula for the production of  $G^2$  and  $G\tilde{G}$  glueballs with most of the details given in Appendix D-Appendix E-Appendix F.

#### 13.1. Kinematics for the Reggeized limit

For the process  $p(p_1) + p(p_2) \rightarrow p(p_3) + p(p_4) + X(p_5)$  we will set the incoming protons back-to-back

$$p_1 = (E, 0, 0, p) \quad p_2 = (E, 0, 0, -p) \quad p_{i=3,4,5} = (E_i, q_{\perp i}, p_{iz}) \quad (47)$$



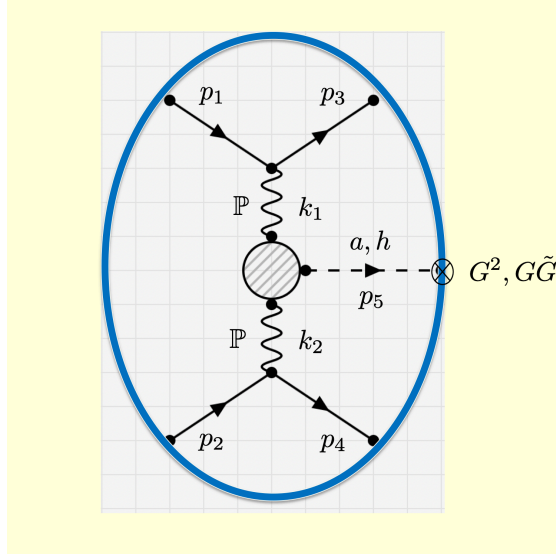


Figure 10: Witten diagram for diffractive  $pp \rightarrow ppX$  with  $X = (a, f) \equiv (G, \tilde{G})$  for the sphaleron at the boundary

with longitudinal fractions  $p_{3z} = x_1 p$  and  $p_{4z} = -x_2 p$  for the outgoing protons. The transverse momenta in the azimuthal plane are 2-vectors

$$q_{\perp 3} = (q_3 \cos \theta_3, q_3 \sin \theta_3) \quad q_{\perp 4} = (q_4 \cos \theta_4, q_4 \sin \theta_4) \quad (48)$$

The Mandelstam kinematics suggests five invariants

$$s = (p_1 + p_2)^2 \quad t_1 = (p_1 - p_3)^2 \quad t_2 = (p_2 - p_4)^2 \quad s_1 = (p_3 + p_5)^2 \quad s_2 = (p_4 + p_5)^2 \quad (49)$$

which are reduced to four by azimuthal symmetry. We will choose the four invariants as  $t_1, t_2$ , the relative azimuthal angle  $\theta_{34} = \theta_4 - \theta_3$ , and the relative momentum fraction  $x_F = x_1 - x_2$ . Following [7], the Reggeized limit is characterized by large  $\sqrt{s}$  and small scattering or azimuthal angles,

$$s \gg s_1, s_2 \gg -t_1, -t_2, m_N^2 \quad \text{and fixed} \quad \mu = \frac{s_1 s_2}{s} \quad (50)$$

with the simplified kinematics

$$s_{1,2} \approx \sqrt{\mu s} \quad t_{1,2} \approx -q_{\perp 3,4}^2 \quad \mu \approx p_5^2 + t_1 + t_2 + 2\sqrt{t_1 t_2} \cos \theta_{34} \quad (51)$$

In this limit and using (51), the differential cross section for  $pp \rightarrow pp0\mp$  is dominated by  $x_F \approx 0$  [7], and reads

$$\frac{d\sigma_{\mp}}{d\theta_{34} dt_1 dt_2} \approx \frac{1}{16\pi^4 s^2} \ln\left(\frac{s}{\mu}\right) \frac{1}{4} \sum_{\text{spin}} \left| \mathcal{A}_{pp \rightarrow pp0\mp} \right|^2 \quad (52)$$

for the production amplitudes (G.12) and (G.13) respectively. We now make explicit the production amplitude for scalar and pseudoscalar production.

### 13.2. Differential cross section: $G\tilde{G}$

The main elements entering the Witten amplitude in Fig 10 for  $pp \rightarrow pp0-$  through **PP** fusion are detailed in the Appendices Appendix D-Appendix E-Appendix F, and specialized to the soft wall model in a slab of AdS<sub>5</sub>. Other models in AdS<sub>5</sub> yield similar results. The ensuing squared spin-averaged amplitude entering (52) is

$$\begin{aligned}
& \frac{1}{4} \sum_{\text{spins}} \left| \mathcal{A}_{pp \rightarrow pp0-} \right|^2 = \frac{16}{4} A^2(t_1) A^2(t_2) \\
& \times \left[ \left( \frac{\lambda}{\pi^2} + 1 \right)^2 \left( \frac{\sqrt{\lambda}}{2\pi} \left( \gamma + \frac{\pi}{2} \right) \right)^4 \frac{e^{-\sqrt{\lambda}(\gamma+\pi/2)^2(1/\ln(s_1/\tilde{\kappa}_N^2)+1/\ln(s_2/\tilde{\kappa}_N^2))}}{(\ln(s_1/\tilde{\kappa}_N^2)\ln(s_2/\tilde{\kappa}_N^2))^3} \left( \frac{s_1}{\tilde{\kappa}_N^2} \right)^{2(\alpha_{\mathbb{P}}(t_1)-2)} \left( \frac{s_2}{\tilde{\kappa}_N^2} \right)^{2(\alpha_{\mathbb{P}}(t_2)-2)} \right] \\
& \times \left[ \left( B_1^-(t_1, t_2)\eta_{\beta\bar{\beta}} + B_2^-(t_1, t_2)k_{2\beta}k_{1\bar{\beta}} \right) \epsilon_{\alpha\bar{\alpha}\gamma\delta} k_1^\gamma k_2^\delta \right] \\
& \times \left[ \left( B_1^-(t_1, t_2)\eta_{\beta\bar{\beta}} + B_2^-(t_1, t_2)k_{2\beta}k_{1\bar{\beta}} \right) \epsilon_{\alpha\bar{\alpha}\gamma\delta} k_1^\gamma k_2^\delta \right] \\
& \times \left[ p^\alpha p^\beta p_{\bar{\alpha}} p_{\bar{\beta}} + \frac{1}{16} \left( t_1 \eta_{\alpha\bar{\alpha}} p_\beta p_{\bar{\beta}} + t_1 \eta_{\alpha\bar{\beta}} p_\beta p_{\bar{\alpha}} + t_1 \eta_{\beta\bar{\alpha}} p_\alpha p_{\bar{\beta}} + (t_1 \eta_{\beta\bar{\beta}} - k_{1\beta} k_{1\bar{\beta}}) p_\alpha p_{\bar{\alpha}} \right) \right] \\
& \times \left[ \underline{p}^{\bar{\alpha}} \underline{p}^{\bar{\beta}} \underline{p}_{\bar{\alpha}} \underline{p}_{\bar{\beta}} + \frac{1}{16} \left( t_2 \eta_{\bar{\alpha}\bar{\alpha}} \underline{p}_{\bar{\beta}} \underline{p}_{\bar{\beta}} + t_2 \eta_{\bar{\alpha}\bar{\beta}} \underline{p}_{\bar{\beta}} \underline{p}_{\bar{\alpha}} + t_2 \eta_{\bar{\beta}\bar{\alpha}} \underline{p}_{\bar{\alpha}} \underline{p}_{\bar{\beta}} + (t_2 \eta_{\bar{\beta}\bar{\beta}} - k_{1\bar{\beta}} k_{1\bar{\beta}}) \underline{p}_{\bar{\alpha}} \underline{p}_{\bar{\alpha}} \right) \right] \quad (53)
\end{aligned}$$

with the vertex

$$2B_1^-(t_1, t_2) - \mu B_2^-(t_1, t_2) = 4 \left( \mathbf{C}_1^- - \mathbf{C}_2^- \sqrt{t_1 t_2} \cos \theta_{34} \right) \quad (54)$$

and  $\mathbf{C}_{1,2}^-$  given in (F.13-F.14) for the soft-wall model. Here, the Pomeron trajectory is the Reggeized graviton trajectory

$$\alpha_{\mathbb{P}}(t) = \alpha_{\mathbb{P}}(0) + \frac{\alpha'}{2} t \equiv 2 - \frac{2}{\sqrt{\lambda}} + \frac{\alpha'}{2} t \quad (55)$$

after restoring the t-dependence, with  $\alpha' = l_s^2$  (the squared string length). For simplicity we have set  $\lambda \rightarrow \infty$  in the A-form factors in (53), i.e.  $A(j_0 \rightarrow 2, k) \equiv A(t)$ , although this can be relaxed. A similar observation was made originally in [1] (instantons) and more recently in [7] (holography) for the double diffractive production of  $\eta, \eta'$ .

We recall that for the nucleon as a Dirac fermion, the energy momentum tensor is characterized by three invariant form factors

$$\langle p_2 | T^{\mu\nu}(0) | p_1 \rangle = \bar{u}(p_2) \left( A(k) \gamma^{(\mu} p^{\nu)} + B(k) \frac{i p^{(\mu} \sigma^{\nu)\alpha} k_\alpha}{2m_N} + C(k) \frac{k^\mu k^\nu - \eta^{\mu\nu} k^2}{m_N} \right) u(p_1), \quad (56)$$

with  $p = (p_1 + p_2)/2$  and  $k = p_2 - p_1$ , and the normalization  $\langle p | T_\mu^\mu | p \rangle = 2A(0)m_N^2$ . In Appendix Appendix D,  $A(t)$  is given explicitly for the soft wall model, which is found to be well parametrized by the dipole form [52]

$$A(k) = \frac{A(0)}{\left(1 + \frac{K^2}{m_A^2}\right)^2} = \frac{A(0)}{\left(1 - \frac{t}{m_A^2}\right)^2} \equiv A(t) \quad (57)$$

with  $m_A = 1.124$  GeV. It compares well with the reported lattice value  $m_{A, \text{lattice}} = 1.13$  GeV by the MIT group [53], for  $A(0) = 0.58$ . The gravitational form factor  $A(k)$  is saturated by the  $2^{++}$  glueball trajectory

without any quark mixing, essentially a quenched result. The holographic C-term  $C(k) = -4A(k)$  is also in good agreement with the lattice results. The holographic B-term is found to vanish which is consistent with the lattice findings. Note that (57) corresponds to a squared gravitational radius of the nucleon as a bulk Dirac fermion

$$\langle r_G^2 \rangle = 6 \left( \frac{d \log A(t)}{dt} \right)_{t=0} = (0.61 \text{ fm})^2 \quad (58)$$

which is smaller than the nucleon squared charge radius  $\langle r_C^2 \rangle = (0.831 \text{ fm})^2$  [54].

In the Reggeized limit, the dominant contributions in the last two brackets stem from the first two terms with  $p^2, \underline{p}^2 \sim s$  as the lead gravitational coupling to the energy-momentum tensor, with the result

$$\begin{aligned} & \frac{1}{4} \sum_{\text{spins}} \left| \mathcal{A}_{pp \rightarrow pp0-} \right|^2 \approx \frac{1}{4} A^2(t_1) A^2(t_2) \\ & \times \left[ \left( \frac{\lambda}{\pi^2} + 1 \right)^2 \left( \frac{\sqrt{\lambda}}{2\pi} \left( \gamma + \frac{\pi}{2} \right) \right)^4 \frac{e^{-\sqrt{\lambda}(\gamma+\pi/2)^2(1/\ln(s_1/\tilde{\kappa}_N^2)+1/\ln(s_2/\tilde{\kappa}_N^2))}}{(\ln(s_1/\tilde{\kappa}_N^2)\ln(s_2/\tilde{\kappa}_N^2))^3} \left( \frac{s_1}{\tilde{\kappa}_N^2} \right)^{2(\alpha_{\mathbb{P}}(t_1)-2)} \left( \frac{s_2}{\tilde{\kappa}_N^2} \right)^{2(\alpha_{\mathbb{P}}(t_2)-2)} \right] \\ & \times s^4 t_1 t_2 \left( 2B_1^-(t_1, t_2) - \mu B_2^-(t_1, t_2) \right)^2 \sin^2 \theta_{34} \end{aligned} \quad (59)$$

The corresponding differential cross section is

$$\begin{aligned} \frac{d\sigma_-}{d\theta_{34} dt_1 dt_2} & \approx \frac{1}{(8\pi)^4} A^2(t_1) A^2(t_2) t_1 t_2 \left( 2B_1^-(t_1, t_2) - \mu B_2^-(t_1, t_2) \right)^2 \sin^2 \theta_{34} \\ & \times \left[ \left( \frac{\lambda}{\pi^2} + 1 \right)^2 \left( \frac{\sqrt{\lambda}}{2\pi} \left( \gamma + \frac{\pi}{2} \right) \right)^4 \frac{e^{-\sqrt{\lambda}(\gamma+\pi/2)^2(1/\ln(s_1/\tilde{\kappa}_N^2)+1/\ln(s_2/\tilde{\kappa}_N^2))}}{(\ln(s_1/\tilde{\kappa}_N^2)\ln(s_2/\tilde{\kappa}_N^2))^3} \right. \\ & \left. \times \left[ \left( \frac{s_1}{\tilde{\kappa}_N^2} \right)^{2(\alpha_{\mathbb{P}}(t_1)-2)} \left( \frac{s_2}{\tilde{\kappa}_N^2} \right)^{2(\alpha_{\mathbb{P}}(t_2)-2)} \right] \left[ s^2 \ln \left( \frac{s}{\mu} \right) \right] \right] \end{aligned} \quad (60)$$

For  $s_{1,2} \sim \sqrt{\mu s}$  and fixed  $\mu$  in the Reggeized limit, (60) asymptotes

$$\ln s \left[ \left( \frac{e^{-\#\sqrt{\lambda}/\ln s}}{(\ln s)^{\frac{3}{2}}} \right)^2 s^{1+\frac{1}{2}(\alpha_{\mathbb{P}}(t_1)+\alpha_{\mathbb{P}}(t_2)-4)} \right]^2 \quad (61)$$

with the first logarithm accounting for the  $x_F \sim 0$  phase space enhancement [7], and the remainder for the 2-Pomeron fusion exchange with its holographic diffusive signature in  $5 - 2 = 3$  transverse directions. The rise in  $s$  can be tamed through the Eikonalization of the exchange.

Finally, we note the transverse plane dependence on  $\sin^2 \theta_{34}$  of the differential cross section (also through  $\mu$  in (51)) as inherited from the abnormal parity nature of the Chern-Simons vertex (F.8) at the origin of the pseudo-scalar emission in bulk. The diffractive emission of the pseudo-scalar glueball is strongly anisotropic in the transverse plane.

### 13.3. Differential cross section: $G^2$

A similar reasoning applies for the spin-averaged squared amplitude for  $pp \rightarrow pp0+$  which reads

$$\begin{aligned}
& \frac{1}{4} \sum_{\text{spins}} \left| \mathcal{A}_{pp \rightarrow pp0+} \right|^2 = \frac{16}{4} A^2(t_1) A^2(t_2) \\
& \times \left[ \left( \frac{\lambda}{\pi^2} + 1 \right)^2 \left( \frac{\sqrt{\lambda}}{2\pi} \left( \gamma + \frac{\pi}{2} \right) \right)^4 \frac{e^{-\sqrt{\lambda}(\gamma+\pi/2)^2(1/\ln(s_1/\tilde{\kappa}_N^2)+1/\ln(s_2/\tilde{\kappa}_N^2))}}{(\ln(s_1/\tilde{\kappa}_N^2)\ln(s_2/\tilde{\kappa}_N^2))^3} \left( \frac{s_1}{\tilde{\kappa}_N^2} \right)^{2(\alpha_{\mathbb{F}}(t_1)-2)} \left( \frac{s_2}{\tilde{\kappa}_N^2} \right)^{2(\alpha_{\mathbb{F}}(t_2)-2)} \right] \\
& \times \left[ B^+(t_1, t_2, p_5^2) \eta_{\alpha\bar{\alpha}} \eta_{\beta\bar{\beta}} \right] \times \left[ B^+(t_1, t_2, p_5^2) \eta_{\underline{\alpha}\bar{\alpha}} \eta_{\underline{\beta}\bar{\beta}} \right] \\
& \times \left[ p^\alpha p^\beta p^{\underline{\alpha}} p^{\underline{\beta}} + \frac{1}{16} \left( t_1 \eta_{\alpha\bar{\alpha}} p_\beta p_{\bar{\beta}} + t_1 \eta_{\alpha\bar{\beta}} p_\beta p_{\bar{\alpha}} + t_1 \eta_{\beta\bar{\alpha}} p_\alpha p_{\bar{\beta}} + (t_1 \eta_{\beta\bar{\beta}} - k_{1\beta} k_{1\bar{\beta}}) p_\alpha p_{\bar{\alpha}} \right) \right] \\
& \times \left[ \underline{p}^{\bar{\alpha}} \underline{p}^{\bar{\beta}} \underline{p}^{\bar{\alpha}} \underline{p}^{\bar{\beta}} + \frac{1}{16} \left( t_2 \eta_{\bar{\alpha}\bar{\alpha}} \underline{p}_\beta \underline{p}_{\bar{\beta}} + t_2 \eta_{\bar{\alpha}\bar{\beta}} \underline{p}_\beta \underline{p}_{\bar{\alpha}} + t_2 \eta_{\bar{\beta}\bar{\alpha}} \underline{p}_\alpha \underline{p}_{\bar{\beta}} + (t_2 \eta_{\bar{\beta}\bar{\beta}} - k_{1\bar{\beta}} k_{1\bar{\beta}}) \underline{p}_\alpha \underline{p}_{\bar{\alpha}} \right) \right] \tag{62}
\end{aligned}$$

Again, in the Reggeized limit, the dominant contributions in the last two brackets stem from the first two terms with  $p^2, \underline{p}^2 \sim s$ , with the result

$$\begin{aligned}
& \frac{d\sigma_+}{d\theta_{34} dt_1 dt_2} \approx \frac{1}{(8\pi)^4} A^2(t_1) A^2(t_2) B^{+2}(t_1, t_2, p_5^2) \\
& \times \left[ \left( \frac{\lambda}{\pi^2} + 1 \right)^2 \left( \frac{\sqrt{\lambda}}{2\pi} \left( \gamma + \frac{\pi}{2} \right) \right)^4 \frac{e^{-\sqrt{\lambda}(\gamma+\pi/2)^2(1/\ln(s_1/\tilde{\kappa}_N^2)+1/\ln(s_2/\tilde{\kappa}_N^2))}}{(\ln(s_1/\tilde{\kappa}_N^2)\ln(s_2/\tilde{\kappa}_N^2))^3} \right] \\
& \times \left[ \left( \frac{s_1}{\tilde{\kappa}_N^2} \right)^{2(\alpha_{\mathbb{F}}(t_1)-2)} \left( \frac{s_2}{\tilde{\kappa}_N^2} \right)^{2(\alpha_{\mathbb{F}}(t_2)-2)} \right] \left[ s^4 \ln \left( \frac{s}{\mu} \right) \right] \tag{63}
\end{aligned}$$

with the scalar vertex  $B^+(t_1, t_2, p_5^2)$

$$B^+(t_1, t_2, p_5^2) = \left( \mathbf{C}_1^+(p_5^2 + (t_1 + t_2)) - 2\mathbf{C}_2^+ - \mathbf{C}_3^+ p_5^2 \right) \tag{64}$$

and  $p_5^2 = m_{0+}^2$  on mass-shell.  $\mathbf{C}_{1,2,3}^+$  are given in (F.5-F.7) for the soft-wall model. Modulo  $\mu$ , the emission of the scalar glueball is isotropic in the transverse plane, in contrast to the pseudo-scalar glueball emission.

## 14. Summary

The subject of this paper – instanton-sphaleron processes, both in QCD and electroweak setting – were at the forefront of the theoretical discussions in the late 1980s. The optimal tunneling path was suggested by Yung [20] and Verbaarschot [21]. The idea to use it to evaluate cross sections was suggested by Ringwald and Khoze [14], as well as Verbaarschot and Shuryak [15]. A more detailed description of the topological landscape and the realization that this path leads to the production of sphalerons came in 2002, from Ref. [12]. The analytic form of a (pure gauge) sphaleron classical explosion was also obtained in that work, with a complementary derivation by us in [22], clarifying the production of fermions. So, from the theoretical perspective, one might think the issue was completely clarified many years ago.

Ringwald and Schrempp [43] put a lot of efforts to identify the instanton-induced reactions in deep-inelastic scattering at HERA. The large  $Q^2$  scale involved, pushes the instantons to be very small, causing the corresponding cross sections to be also small. However, the real problem turned out to be the separation of the “instanton events” from the multi-jet background. The more recent version for the LHC, by Khoze et al [44], relates the instanton size to the fraction of the collision energy, again with a cross section that is strongly decreasing with the invariant mass  $M = \sqrt{s'}$  of the produced cluster. This mechanism was recently revisited using single-diffractive medium cluster production and a more favorable choice of kinematics, but with stringent cuts [55].

While we do not disagree with these approaches, we still think one needs a different experimental strategy. One better starts with smaller clusters, with invariant masses of several GeV, which offer clearly identifiable mesonic and perhaps baryonic final states, which can be related to existing theoretical predictions. The background issue would be helped if instead of min.bias  $pp$  collisions one would use the double diffraction, or **PP** collisions. Last but not least, using gluon-rich but colorless fusing Pomerons, rather than fusing gluonic partons, eliminates the need for color flux tubes and cleans up the stage.

Can it all be done in practice, and if so, *why now?* It looks like LHC has reached certain stage of multiple searches at which all which remains to do is to increase statistics. The search for instanton/sphaleron clusters may not be “beyond the standard model” but is still worth trying.

The double diffractive direction we advocate is in especially nice position. The first roman pot (RP) detectors are installed and running. ATLAS AFP is tuned to a huge mass  $M \sim 1$  TeV, while CMS-TOTEM has carried studies of exclusive reactions at  $M \sim 1$  GeV. The in between region we suggest to explore is still basically “*terra incognita*”. It remained untouched for decades, since the pioneering *UA8* experiment.

Last but not least, the QCD sphalerons and their explosions are close relatives of the electroweak sphalerons. We do not know how one may produce those in the lab, but we do expect them to be very important at the cosmological electroweak transition [56].

**Acknowledgements** This work has been triggered by the CERN workshop ” Topological Effects in the Standard Model: Instantons, Sphalerons and Beyond at LHC”, Dec-2020. We thank its organizers, and especially Matthias Schott, for organizing it and for reviving this field in general. This work is supported by the Office of Science, U.S. Department of Energy under Contract No. DE-FG-88ER40388.

## Appendix A. Some meson couplings used

For completeness, we give here some standard PCAC formulae and their numerical values,

$$K_\pi \equiv \langle 0 | \bar{d} \gamma^5 u | \pi^+ \rangle = i \frac{m_\pi^2 f_\pi}{m_u + m_d} \approx i(500 \text{ MeV})^2 \quad (\text{A.1})$$

$$K_K \equiv \langle 0 | \bar{s} \gamma^5 u | K^+ \rangle = i \frac{m_K^2 f_K}{m_u + m_s} \approx i(523 \text{ MeV})^2 \quad (\text{A.2})$$

The  $\eta, \eta'$  couplings depend on the mixing angle. We will use the same values adopted in [34]

$$\begin{aligned} K_\eta^q &\equiv \langle 0 | \bar{u} \gamma^5 u | \eta \rangle = \langle 0 | \bar{d} \gamma^5 d | \eta \rangle = -i(358 \text{ MeV})^2 \\ K_{\eta'}^q &\equiv \langle 0 | \bar{u} \gamma^5 u | \eta' \rangle = \langle 0 | \bar{d} \gamma^5 d | \eta' \rangle = -i(320 \text{ MeV})^2 \\ K_\eta^s &\equiv \langle 0 | \bar{s} \gamma^5 s | \eta \rangle = i(435 \text{ MeV})^2 \\ K_{\eta'}^s &\equiv \langle 0 | \bar{s} \gamma^5 s | \eta' \rangle = i(481 \text{ MeV})^2 \end{aligned} \quad (\text{A.3})$$

The other issue is to define the  $\bar{s}s$  part of  $\eta, \eta'$  responsible for the observed  $\eta\pi\pi$  and  $\eta'\pi\pi$  decay rates. The  $\eta - \eta'$  mixing has been well researched. In terms of singlet and octet states

$$\begin{aligned} \eta_8 &= \frac{1}{\sqrt{6}}(\bar{u}u + \bar{d}d - 2\bar{s}s) \\ \eta_1 &= \frac{1}{\sqrt{3}}(\bar{u}u + \bar{d}d + \bar{s}s) \end{aligned} \quad (\text{A.4})$$

the standard definition of the mixing is

$$\begin{aligned} \eta' &= \sin(\theta_p)\eta_8 + \cos(\theta_p)\eta_1 \\ \eta &= \cos(\theta_p)\eta_8 - \sin(\theta_p)\eta_1 \end{aligned} \quad (\text{A.5})$$

Using the mixing angle  $\theta_p \approx -14.6^\circ$ , one finds that the ratio of the  $\bar{s}s$  probabilities (squares of amplitudes) is

$$\frac{ss_{\eta'}}{ss_{\eta}} = \left( \frac{0.764}{0.644} \right)^2 = 1.40 \quad (\text{A.6})$$

## Appendix B. Instanton-induced $uuddss$ interactions

In this Appendix we outline the general structure of the induced 't Hooft vertex for multi-quark states. In particular, we show the explicit steps that lead to the 6-quark vertex both in the color bleached and bleached form. its generalization to 8- and 10-quark states follows. An alternative but tedious formula involving color averaging over the color moduli with also be discussed which can be generalized to even higher multi-quark states.

### Appendix B.1. Details of the color-spin reduction

The momentum-space kernel for the LSZ reduced zero-mode propagator in the instanton background reads

$$L \equiv \left[ \frac{(p^2 \varphi'(p))_0^2}{m\rho} \right] \left[ \frac{1}{8} U(\delta_{\mu\nu} + i\bar{\eta}_{\mu\nu}^a \tau^a) U^\dagger \times \gamma_\mu \gamma_\nu \right] \frac{1 - \gamma_5}{2} \quad (\text{B.1})$$

in the zero momentum limit  $(p^2 \varphi'(p))_0 \equiv \sqrt{C}$ . The 6-quark  $uuddss$  vertex stemming from (B.1) follows from averaging over the color matrices  $U$  the product

$$\begin{aligned} \int dU [L]^3 &= \left[ \frac{1}{8} U(\delta_{\alpha\beta} + i\bar{\eta}_{\alpha\beta}^a \tau^a) U^\dagger \times \gamma_\alpha \gamma_\beta \right] \\ &\times \left[ \frac{1}{8} U(\delta_{\mu\nu} + i\bar{\eta}_{\mu\nu}^b \tau^b) U^\dagger \times \gamma_\mu \gamma_\nu \right] \times \left[ \frac{1}{8} U(\delta_{\lambda\tau} + i\bar{\eta}_{\lambda\tau}^c \tau^c) U^\dagger \times \gamma_\lambda \gamma_\tau \right] \end{aligned} \quad (\text{B.2})$$

using the identity [37]

$$\begin{aligned} \int dU [U_i^a U_b^\dagger j^j]^3 &= \left[ \frac{1}{N_c} \delta_{b_1}^{a_1} \delta_{i_1}^{j_1} \mathbf{1}_1 \right] \left[ \frac{1}{N_c} \delta_{b_2}^{a_2} \delta_{i_2}^{j_2} \mathbf{1}_2 \right] \left[ \frac{1}{N_c} \delta_{b_3}^{a_3} \delta_{i_3}^{j_3} \mathbf{1}_3 \right] \\ &+ \left( \left[ \frac{1}{N_c} \delta_{b_1}^{a_1} \delta_{i_1}^{j_1} \mathbf{1}_1 \right] \left[ \frac{1}{4(N_c^2 - 1)} [\lambda_2^A]_{b_2}^{a_2} [\lambda_3^A]_{b_3}^{a_3} [\lambda_2^B]_{i_2}^{j_2} [\lambda_3^B]_{i_3}^{j_3} \right] + 2 \text{ perm.} \right) \\ &+ \left( \frac{N_c}{8(N_c^2 - 1)(N_c^2 - 4)} \left[ d^{ABC} ([\lambda_1^A]_{b_1}^{a_1} [\lambda_2^B]_{b_2}^{a_2} [\lambda_3^C]_{b_3}^{a_3}) \left[ d^{IJK} ([\lambda_1^I]_{i_1}^{j_1} [\lambda_2^J]_{i_2}^{j_2} [\lambda_3^K]_{i_3}^{j_3}) \right] \right) \right) \\ &+ \left( \frac{1}{8N_c(N_c^2 - 1)} \left[ f^{ABC} ([\lambda_1^A]_{b_1}^{a_1} [\lambda_2^B]_{b_2}^{a_2} [\lambda_3^C]_{b_3}^{a_3}) \left[ f^{IJK} ([\lambda_1^I]_{i_1}^{j_1} [\lambda_2^J]_{i_2}^{j_2} [\lambda_3^K]_{i_3}^{j_3}) \right] \right) \right) \end{aligned} \quad (\text{B.3})$$

which follows from the projection onto the color singlet channel. The result after some algebra is

$$\begin{aligned} \left[ \frac{C}{m\rho N_c} \right]^3 &\left( UDS + \frac{N_c(N_c - 2)}{4(N_c^2 - 1)} \left[ U^A D^A S + U^A D S^A + U D^A S^A \right] \right. \\ &\quad \left. - \frac{N_c^2}{16(N_c^2 - 1)} \left[ U_{\mu\nu}^A D_{\mu\nu}^A S + U_{\mu\nu}^A D S_{\mu\nu}^A + U D_{\mu\nu}^A S_{\mu\nu}^A \right] \right) \\ &\quad - \frac{N_c^3(N_c - 2)}{96(N_c^2 - 1)(N_c^2 - 4)} d^{ABC} \left[ U_{\mu\nu}^A D_{\mu\nu}^B S^C + U_{\mu\nu}^A D^B S_{\mu\nu}^C + U^A D_{\mu\nu}^B S_{\mu\nu}^C \right] \\ &\quad \left. + \frac{N_c^2(N_c - 2)}{8(N_c^2 - 1)(N_c + 2)} d^{ABC} U^A D^B S^C - \frac{N_c^2}{32(N_c^2 - 1)} i f^{ABC} U_{\mu\nu}^A D_{\nu\rho}^B S_{\rho\mu}^C \right) \end{aligned} \quad (\text{B.4})$$

where we have defined

$$\begin{aligned}
U &= \bar{u}_R u_L & U^A &= \bar{u}_R \lambda^A u_L & U_{\mu\nu}^A &= \bar{u}_R \lambda^A \gamma_\mu \gamma_\nu u_L \\
D &= \bar{d}_R d_L & D^A &= \bar{d}_R \lambda^A d_L & D_{\mu\nu}^A &= \bar{d}_R \lambda^A \gamma_\mu \gamma_\nu d_L \\
S &= \bar{s}_R s_L & S^A &= \bar{s}_R \lambda^A s_L & S_{\mu\nu}^A &= \bar{s}_R \lambda^A \gamma_\mu \gamma_\nu s_L
\end{aligned} \tag{B.5}$$

Throughout in the notation  $\gamma_\mu \gamma_\nu$  the condition  $\mu < \nu$  is subsumed. (B.3) was originally derived in [57] for  $N_c = 3$ .

(B.4) can be considerably reduced by successive Fierzing to bleach the color and bring it to a determinantal form typical of instanton induced interactions that are manifestly  $SU(N_f)$  symmetric but  $U(1_f)$  violating. Since the procedure is considerably lengthy, we will show how the Fierzing works for the typical blocks in (B.4).

Consider the typical colored scalar block in (B.4)

$$\begin{aligned}
U^A D^A &\equiv \bar{u}_R \lambda^A u_L \bar{d}_R \lambda^A d_L \\
&= \bar{u}_{Ra} u_{Lb} \bar{d}_{Rc} d_{Ld} [\lambda^A]^{ab} [\lambda^A]^{cd} = 2\bar{u}_{Ra} u_{Lb} \bar{d}_{Rb} d_{La} - \frac{2}{N_c} \bar{u}_R u_L \bar{d}_R d_L \\
&= -\frac{2}{N_c} \bar{u}_R u_L \bar{d}_R d_L - \bar{u}_R d_L \bar{d}_R u_L + \frac{1}{4} \bar{u}_R \gamma_\mu \gamma_\nu d_L \bar{d}_R \gamma_\mu \gamma_\nu u_L
\end{aligned} \tag{B.6}$$

where we made use of the color identity in the second line

$$[\lambda^A]^{ab} [\lambda^A]^{cd} = 2\delta^{ad} \delta^{bc} - \frac{2}{N_c} \delta^{ab} \delta^{cd} \tag{B.7}$$

and the Fierz re-arrangement in the third line

$$\bar{u}_{Ra} u_{Lb} \bar{d}_{Rb} d_{La} = -\frac{1}{2} \bar{u}_R d_L \bar{d}_R u_L + \frac{1}{8} \bar{u}_R \gamma_\mu \gamma_\nu d_L \bar{d}_R \gamma_\mu \gamma_\nu u_L \tag{B.8}$$

The same procedure carries for the colored tensor block with the result

$$\begin{aligned}
U_{\mu\nu}^A D_{\mu\nu}^A &\equiv \bar{u}_R \lambda^A \gamma_\mu \gamma_\nu u_L \bar{d}_R \lambda^A \gamma_\mu \gamma_\nu d_L \\
&= -\frac{2}{N_c} \bar{u}_R \gamma_\mu \gamma_\nu u_L \bar{d}_R \gamma_\mu \gamma_\nu d_L + 12\bar{u}_R d_L \bar{d}_R u_L + \bar{u}_R \gamma_\mu \gamma_\nu d_L \bar{d}_R \gamma_\mu \gamma_\nu u_L
\end{aligned} \tag{B.9}$$

using the Fierz re-arrangement

$$\bar{u}_{Ra} \gamma_\mu \gamma_\nu u_{Lb} \bar{d}_{Rb} \gamma_\mu \gamma_\nu d_{La} = 6\bar{u}_R d_L \bar{d}_R u_L + \frac{1}{2} \bar{u}_R \gamma_\mu \gamma_\nu d_L \bar{d}_R \gamma_\mu \gamma_\nu u_L \tag{B.10}$$

The bleaching of color from the contributions involving the structure factors  $f^{ABC}$  and  $d^{ABC}$  can be simplified by noting the respective identities

$$i f^{ABC} [\lambda^A]^{ab} [\lambda^B]^{cd} [\lambda^C]^{ef} = 2 \left( \delta^{ad} \delta^{cf} \delta^{eb} - \delta^{af} \delta^{cb} \delta^{ed} \right) \tag{B.11}$$

and

$$\begin{aligned}
d^{ABC}[\lambda^A]^{ab}[\lambda^B]^{cd}[\lambda^C]^{ef} = & 2\left(\delta^{ad}\delta^{cf}\delta^{eb} + \delta^{af}\delta^{cb}\delta^{ed}\right) - \frac{4}{N_c^2}\delta^{ab}\delta^{cd}\delta^{ef} \\
& - \frac{2}{N_c}\left(\delta^{ab}[\lambda^A]^{cd}[\lambda^A]^{ef} + \delta^{cd}[\lambda^A]^{ab}[\lambda^A]^{ef} + \delta^{ef}[\lambda^A]^{ab}[\lambda^A]^{cd}\right) \quad (\text{B.12})
\end{aligned}$$

(B.11-B.12) can be established by Fierzing in color and using the identities

$$\begin{aligned}
\frac{1}{8}d^{ABC}[\lambda^A]_b^a[\lambda^B]_c^b[\lambda^C]_d^c &= \frac{N_c^2 - 4}{2N_c}C_F\delta_d^a \\
\frac{1}{8}f^{ABC}[\lambda^A]_b^a[\lambda^B]_c^b[\lambda^C]_d^c &= \frac{i}{2}N_cC_F\delta_d^a \quad (\text{B.13})
\end{aligned}$$

with  $C_F = (N_c^2 - 1)/2N_c$  the Casimir in the fundamental representation. (B.12) can be totally color reduced using (B.7). Inserting (B.6-B.9-B.11-B.12) in (B.4) yield (23) after lengthy algebraic re-arrangements. Note that in (23) we are still using the notation  $Q_{\mu\nu}$  but with  $\sigma_{\mu\nu}$  instead of  $\gamma_\mu\gamma_\nu$  with  $\mu < \nu$  subsumed.

### Appendix B.2. Alternative form

An alternative form for the 6-quark 't Hooft vertex, can be reached by reconsidering the full LSZ reduced amplitude in Weyl notations

$$\begin{aligned}
\left[\frac{n_I}{2}\right]_\rho & \int \frac{d^4k_1}{(2\pi)^4} \frac{d^4k_2}{(2\pi)^4} \frac{d^4p_1}{(2\pi)^4} \frac{d^4p_2}{(2\pi)^4} \frac{d^4q_1}{(2\pi)^4} \frac{d^4q_2}{(2\pi)^4} \left[ (2\pi)^4 \delta^4(k_1 + p_1 + q_1 - k_2 - p_2 - q_2) \right. \\
& \times \left[ \left\langle u_R^\dagger(k_2)k_2 \left[ \sqrt{2}\varphi'(k_2)\hat{k}_2\epsilon U \right] \frac{1}{m} \left[ \sqrt{2}\varphi'(k_1)U^\dagger\epsilon\hat{k}_1 \right] k_1 u_L(k_1) \right. \right. \\
& \quad \times d_R^\dagger(p_2)p_2 \left[ \sqrt{2}\varphi'(p_2)\hat{p}_2\epsilon U \right] \frac{1}{m} \left[ \sqrt{2}\varphi'(p_1)U^\dagger\epsilon\hat{p}_1 \right] p_1 d_L(p_1) \\
& \quad \left. \left. \times s_R^\dagger(q_2)q_2 \left[ \sqrt{2}\varphi'(q_2)\hat{q}_2\epsilon U \right] \frac{1}{m} \left[ \sqrt{2}\varphi'(q_1)U^\dagger\epsilon\hat{q}_1 \right] q_1 s_L(q_1) \right\rangle_U \right] + L \leftrightarrow R \quad (\text{B.14})
\end{aligned}$$

after averaging over the instanton Z-position in 4-Euclidean space, without taking the zero momentum limit as in (B.1). The left zero mode in the instanton background in momentum space is

$$\psi_{iI}^\alpha(p) = \sqrt{2}\varphi'(p)(\hat{p}\epsilon U)_i^\alpha \quad \varphi'(p) = \pi\rho^2 \left( I_0 K_0 - I_1 K_1 \right)' (z = \rho p/2) \quad (\text{B.15})$$

in terms of which (B.14) reads

$$\begin{aligned}
\left[\frac{n_I}{2}\right]_\rho & \int \frac{d^4k_1}{(2\pi)^4} \frac{d^4k_2}{(2\pi)^4} \frac{d^4p_1}{(2\pi)^4} \frac{d^4p_2}{(2\pi)^4} \frac{d^4q_1}{(2\pi)^4} \frac{d^4q_2}{(2\pi)^4} \left[ (2\pi)^4 \delta^4(k_1 + p_1 + q_1 - k_2 - p_2 - q_2) \right. \\
& \times \left[ \frac{1}{m^3} (2k_1 k_2 \varphi'(k_1) \varphi'(k_2)) (2p_1 p_2 \varphi'(p_1) \varphi'(p_2)) (2q_1 q_2 \varphi'(q_1) \varphi'(q_2)) \right] \\
& \times \left\langle \left[ u_R^\dagger(k_2)\epsilon U \right] \left[ U^\dagger\epsilon u_L(k_1) \right] \left[ d_R^\dagger(p_2)\epsilon U \right] \left[ U^\dagger\epsilon d_L(p_1) \right] \left[ s_R^\dagger(q_2)\epsilon U \right] \left[ U^\dagger\epsilon s_L(q_1) \right] \right\rangle_U + L \leftrightarrow R \quad (\text{B.16})
\end{aligned}$$

The color bracket is explicitly



$$\begin{aligned}
& \left\langle U_{c_1}^{a_1} U_{d_1}^{\dagger b_1} U_{c_2}^{a_2} U_{d_2}^{\dagger b_2} U_{c_3}^{a_3} U_{d_3}^{\dagger b_3} \right\rangle_U \left[ \epsilon^{i_1 c_1} \epsilon_{j_1 b_1} \epsilon^{i_2 c_2} \epsilon_{j_2 b_2} \epsilon^{i_3 c_3} \epsilon_{j_3 b_3} \right] \\
& \times \left[ u_{R a_1 i_1}^{\dagger}(k_2) u_L^{d_1 j_1}(k_1) d_{R a_2 i_2}^{\dagger}(p_2) d_L^{d_2 j_2}(p_1) s_{R a_3 i_3}^{\dagger}(q_2) s_L^{d_3 j_3}(q_1) \right]
\end{aligned} \tag{B.17}$$

The color averaging over the unitary matrices can be written in terms of the Weingarten coefficients

$$\begin{aligned}
& \left\langle U_{c_1}^{a_1} U_{d_1}^{\dagger b_1} U_{c_2}^{a_2} U_{d_2}^{\dagger b_2} U_{c_3}^{a_3} U_{d_3}^{\dagger b_3} \right\rangle_U = \\
& \frac{(N_c^2 - 2)}{N_c(N_c^2 - 1)(N_c^2 - 4)} \sum_{n=1}^{3!} \delta_{(d_1 d_2 d_3)_n}^{a_1 a_2 a_3} \delta_{(b_1 b_2 b_3)_n}^{c_1 c_2 c_3} \\
& - \frac{1}{(N_c^2 - 1)(N_c^2 - 4)} \sum_{n=1}^{3!} \delta_{(d_1 d_2 d_3)_n}^{a_1 a_2 a_3} \left( \delta_{(b_2 b_1 b_3)_n}^{c_1 c_2 c_3} + \delta_{(b_1 b_3 b_2)_n}^{c_1 c_2 c_3} + \delta_{(b_3 b_2 b_1)_n}^{c_1 c_2 c_3} \right) \\
& + \frac{2}{N_c(N_c^2 - 1)(N_c^2 - 4)} \sum_{n=1}^{3!} \delta_{(d_1 d_2 d_3)_n}^{a_1 a_2 a_3} \left( \delta_{(b_3 b_1 b_2)_n}^{c_1 c_2 c_3} + \delta_{(b_2 b_3 b_1)_n}^{c_1 c_2 c_3} \right)
\end{aligned} \tag{B.18}$$

The short-hand notation

$$\delta_{(d_1 d_2 d_3)_n}^{a_1 a_2 a_3} \equiv \sum_{n=1}^{3!} \left( \delta_{d_1}^{a_1} \delta_{d_2}^{a_2} \delta_{d_3}^{a_3} + \text{perm.} \right) \tag{B.19}$$

refers to the product of three kroneckers in the sum over the  $n!$  permutations of the permutation group  $S_3$ . For completeness, we note the analogous relations for lower color averagings for two flavors

$$\begin{aligned}
& \left\langle U_{c_1}^{a_1} U_{d_1}^{\dagger b_1} U_{c_2}^{a_2} U_{d_2}^{\dagger b_2} \right\rangle_U = \\
& \frac{1}{N_c^2 - 1} \sum_{n=1}^{2!} \delta_{(d_1 d_2)_n}^{a_1 a_2} \delta_{(b_1 b_2)_n}^{c_1 c_2} - \frac{1}{N_c(N_c^2 - 1)} \sum_{n=1}^{2!} \delta_{(d_1 d_2)_n}^{a_1 a_2} \delta_{(b_2 b_1)_n}^{c_1 c_2}
\end{aligned} \tag{B.20}$$

and the well known one for one flavor

$$\left\langle U_c^a U_d^{\dagger b} \right\rangle_U = \frac{1}{N_c} \delta_d^a \delta_b^c \tag{B.21}$$

## Appendix C. Exploding quark modes in Sphaleron background

In so far, we have extracted the sphaleron-six-quark vertex using the  $O(4)$  exact zero modes in a self-dual instanton (anti-instanton) background. While at  $t = 0$  this is the case, as  $t > 0$  the zero modes become real and turn to  $O(3)$  exploding quark modes as we discussed in [22]. We now briefly review how these modes are constructed and then substitute them in (46) to generate  $\mathcal{L}(t > 0)$  to describe the final state explosive vertex in the diffractive  $pp \rightarrow ppX$  process,

### Appendix C.1. $O(4)$ and $O(3)$ fermionic zero mode

A Dirac fermion in a general gauge field solves the equation

$$(\partial_\mu - iA_\mu) \gamma_\mu \psi = 0 \tag{C.1}$$

We will use the chiral basis with spin matrices  $\bar{\sigma}_{Ms} = (1, -i\vec{\sigma}_s)$  and

$$\gamma_5 = \begin{pmatrix} 1 & 0 \\ 0 & -1 \end{pmatrix} \quad \gamma_\mu = \begin{pmatrix} 0 & \sigma_{Ms} \\ \bar{\sigma}_{Ms} & 0 \end{pmatrix} \quad (\text{C.2})$$

If we recall that the  $t'$  Hooft symbol satisfies the color identity  $\bar{\sigma}_{Mc}\sigma_{Nc} = \sigma_{ac}\bar{\eta}_{aMN}$  with  $\sigma_{Mc} = (1, -i\vec{\sigma}_c)$ , then the positive chirality mode  $\psi_+$  solves (C.1)

$$\left( \bar{\sigma}_{Ms}\partial_M + \frac{1}{2}\bar{\sigma}_{Ns}\bar{\sigma}_{Nc}\sigma_{Mc}\partial_M F \right) \psi_+ = 0 \quad (\text{C.3})$$

with the spin and color matrices commuting.  $F(\xi(y))$  for an  $O(4)$  symmetric gauge field is given in (7). Note that while writing (C.3) we have added a  $U(1)$  part to the gauge field for notational simplicity, and will remove it in the final answer by inspection. A formal solution to (C.3) is  $(\psi_+)_\mu^a = \varphi\epsilon_\mu^a$  which is a singlet (hedgehog) in color-spin space

$$\sigma_{Ms}\chi_Q = \bar{\sigma}_{Mc}\epsilon \quad \bar{\sigma}_{Ms}\epsilon = \sigma_{Mc}\epsilon \quad (\text{C.4})$$

Inserting (C.4) in (C.3) yields

$$\left( \bar{\sigma}_{Ms}\partial_M + \frac{1}{2}\bar{\sigma}_{Ns}\sigma_{Ns}\bar{\sigma}_{Ms}\partial_M F \right) \varphi\epsilon = 0 \quad (\text{C.5})$$

To remove the redundant  $U(1)$  contribution noted above we use

$$\bar{\sigma}_{Ns}\sigma_{Ns}\epsilon = (1 + (\vec{\sigma}_s)^2)\epsilon \rightarrow (\vec{\sigma}_s)^2\epsilon = 3\epsilon \quad (\text{C.6})$$

after which  $\varphi$  is seen to solve  $\varphi' + \frac{3}{2}F'\varphi = 0$ , hence

$$(\psi_+)_\mu^a(y) = \mathbf{C} e^{-\frac{3}{2}F(\xi(y))} \epsilon_\mu^a \quad (\text{C.7})$$

with

$$\xi(y) = \frac{1}{2} \ln \left( \frac{(t-\rho)^2 + r^2}{(t+\rho)^2 + r^2} \right) \quad (\text{C.8})$$

The overall normalization  $\mathbf{C}$  is fixed by

$$\mathbf{C} = \left| \int_{T_{\frac{1}{2}}} d^4y e^{-3F(\xi(y))} \right|^{-\frac{1}{2}} \quad (\text{C.9})$$

with  $T_{\frac{1}{2}}$  the sphaleron tunneling time. (C.9) is agreement with the result in [22] (see Eq. 22 with the exponent  $2 \rightarrow \frac{3}{2}$  when (C.6) is enforced).

The chiral  $O(3)$  symmetric zero mode follows by applying the off-center inversion (10) in Section 4, onto the  $O(4)$  symmetric zero mode in (C.7). The corresponding transform is

$$\tilde{\psi}_+(x) = \frac{\sigma_\mu^\dagger(y+a)_\mu}{1/(y+a)^2} \psi_+(y) \quad (\text{C.10})$$

or more explicitly ( $r = |\vec{x}|$ )

$$(\tilde{\psi}_+)_\mu^a(t, r) = \frac{8\mathbf{C}\rho^6}{((t+\rho)^2 + r^2)^2} e^{-\frac{3}{2}F(\xi(y))} [((t+\rho) + i\vec{\sigma} \cdot \vec{x}) \epsilon]_\mu^a \quad (\text{C.11})$$

This result is in agreement with the one derived in [22] prior to the analytical continuation to Minkowski space.

## Appendix D. Graviton-nucleon coupling

In bulk, the graviton couples to the Dirac fermion through its energy momentum tensor [58, 52]

$$-\frac{\sqrt{2\kappa^2}}{2} \int d^5x \sqrt{g} h_{\mu\nu} T_F^{\mu\nu} = -\frac{\sqrt{2\kappa^2}}{2} \int d^5x \sqrt{g} \left( \frac{e^{-\phi}}{2g_5^2} \frac{i}{2} z \bar{\Psi} \gamma^\mu \overleftrightarrow{\partial}^\nu \Psi - \eta^{\mu\nu} \mathcal{L}_F \right) \quad (\text{D.1})$$

with typically for the Dirac fermions in the soft-wall model

$$\mathcal{L}_F = \frac{e^{-\phi(z)}}{2g_5^2} \left( \frac{i}{2} \bar{\Psi} e_A^N \Gamma^A (\overrightarrow{D}_N - \overleftarrow{D}_N) \Psi - (M + V(z)) \bar{\Psi} \Psi \right), \quad (\text{D.2})$$

with  $M = \tau - 3$  the anomalous dimension. The potential  $V(z) = \tilde{\kappa}_N^2 z^2$  is added to make the Dirac fermions massive in bulk. Here  $e_A^N = z \delta_A^N$  denotes the inverse vielbein, and the covariant derivatives are defined as

$$\begin{aligned} \overrightarrow{D}_N &= \overrightarrow{\partial}_N + \frac{1}{8} \omega_{NAB} [\Gamma^A, \Gamma^B] \\ \overleftarrow{D}_N &= \overleftarrow{\partial}_N + \frac{1}{8} \omega_{NAB} [\Gamma^A, \Gamma^B] \end{aligned} \quad (\text{D.3})$$

The components of the spin connection are  $\omega_{\mu z\nu} = -\omega_{\nu z\mu} = \frac{1}{2} \eta_{\mu\nu}$ , the Dirac gamma matrices satisfy anti-commutation relation  $\{\Gamma^A, \Gamma^B\} = 2\eta^{AB}$  with the explicit choice  $\Gamma^A = (\gamma^\mu, -i\gamma^5)$ .

In the nucleon as a bulk Dirac fermion, the energy momentum tensor is characterized by the three invariant form factors in (56). For the soft wall model, we have explicitly [58, 52]

$$A(k) = \frac{1}{2} \int dz \sqrt{g} e^{-\phi} z (\psi_R^2(z) + \psi_L^2(z)) \mathcal{H}(k, z) = -\frac{C(k)}{(\alpha z_0 m_N / 2)^2} \quad (\text{D.4})$$

with  $\mathcal{H}(K, z')$  the non-normalizable bulk-to-boundary graviton propagator [59, 60, 61]

$$\begin{aligned} \mathcal{H}(K, z) &= 4z'^4 \Gamma(a_K + 2) U(a_K + 2, 3; 2\tilde{\kappa}_N^2 z^2) = \Gamma(a_K + 2) U(a_K, -1; 2\tilde{\kappa}_N^2 z^2) \\ &= \frac{\Gamma(a_K + 2)}{\Gamma(a_K)} \int_0^1 dx x^{a_K - 1} (1 - x) \exp\left(-\frac{x}{1 - x} (2\tilde{\kappa}_N^2 z^2)\right) \end{aligned} \quad (\text{D.5})$$

and  $a_K = K^2 / 8\tilde{\kappa}_N^2 \geq 0$ . We have used the transformation  $U(m, n; y) = y^{1-n} U(1 + m - n, 2 - n, y)$ . (D.5) satisfies the normalization condition  $\mathcal{H}(0, z') = \mathcal{H}(K, 0) = 1$ . The bulk Dirac fermions  $\Psi(x, z) = \psi_{L,R}(z) e^{-ip \cdot x} u_{L,R}(p)$  are

$$\psi_R(z) = \frac{\tilde{n}_R}{\tilde{\kappa}_N^{\tau-2}} z^{\frac{5}{2}} \xi^{\frac{\tau-2}{2}} L_0^{(\tau-2)}(\xi) \quad \psi_L(z) = \frac{\tilde{n}_L}{\tilde{\kappa}_N^{\tau-1}} z^{\frac{5}{2}} \xi^{\frac{\tau-1}{2}} L_0^{(\tau-1)}(\xi) \quad (\text{D.6})$$

Here  $\xi = \tilde{\kappa}_N^2 z^2$ ,  $\tau = 7/2 - 1/2 = 3$  is the twist parameter, and  $L_n^{(\alpha)}(\xi)$  are the generalized Laguerre polynomials, with

$$\tilde{n}_R = \tilde{n}_L \tilde{\kappa}_N^{-1} \sqrt{\tau - 1} \quad \tilde{n}_L = \tilde{\kappa}_N^\tau \sqrt{2/\Gamma(\tau)}$$

More specifically [58, 52] ( $k^2 = -K^2 = t \leq 0$ )

$$\begin{aligned} A(k) &= A(0) (a_k + 1) \left( - (1 + a_k + 2a_k^2) + 2 (a_k + 2a_k^3) \Phi(-1, 1, a_k) \right) \\ &= A(0) \left( (1 - 2a_k)(1 + a_k^2) + a_k(1 + a_k)(1 + 2a_k^2) \left( \psi\left(\frac{1 + a_k}{2}\right) - \psi\left(\frac{a_k}{2}\right) \right) \right) \end{aligned} \quad (\text{D.7})$$

with  $a_k = k^2/8\tilde{\kappa}_N^2$ , and  $B(0) = 0$ .  $\Phi(-1, 1, a')$  refers to the LerchPhi function, and  $\psi(x)$  refers to the digamma function or harmonic number  $H_x = \psi(x) + \gamma$ . The gravitational form factor  $C(k)$  is proportional to  $A(k)$  modulo a negative overall constant  $-(\alpha z_0 m_N/2)^2 < 0$  which is left undetermined since  $\alpha$  is arbitrary in the tensor decomposition of the graviton [52]. Note that  $\mathcal{H}(k, 0) = \mathcal{H}(0, z)$  is arbitrary (1-point function), so that  $A(0)$  is not fixed in holography.

## Appendix E. Spin-j-nucleon coupling

For diffractive scattering at large  $\sqrt{s}$ , the spin-2 graviton coupling reggeizes to spin-j coupling. The resummed spin-j couplings transmutates to the Pomeron coupling. The generic form of the spin-j coupling is [52]

$$\mathcal{V}_{h\bar{\Psi}\Psi}^{\alpha\beta(TT)}(j, p_1, p_2, k_z) = -\frac{\sqrt{2\kappa^2}}{2} \int dz \sqrt{g} e^{-\phi} \mathcal{H}(j, K, z) \left[ z^{1+2(j-2)} \frac{1}{2} \bar{\Psi}(p_2, z) \gamma^{[\alpha} p^{\beta]} \Psi(p_1, z) z^{-(j-2)} \right] \quad (\text{E.1})$$

where  $\mathcal{H}(j, K, z)$  is the spin-j bulk to boundary space-like propagator. For the pure spin-2 graviton  $h_\mu^\mu = 0$  is traceless, so the coupling to  $\mathcal{L}_F$  in (D.1) drops out. The z-pre-factors in the internal bracket in (E.1) reflect on the spin-j generalization of the energy-momentum tensor (higher twist vertices). For the soft-wall model, (E.1) takes the explicit form

$$\mathcal{V}_{h\bar{\Psi}\Psi}^{\alpha\beta(TT)}(j, p_1, p_2, k_z) = -\sqrt{2\kappa^2} \times g_5^2 A(j, K) \times \frac{1}{2} \bar{u}(p_2) \gamma^{[\alpha} p^{\beta]} u(p_1) \quad (\text{E.2})$$

with

$$\begin{aligned} A(j, K) &= \frac{1}{2g_5^2} \int dz \sqrt{g} e^{-\phi} \mathcal{H}(j, K, z) \left[ z^{1+2(j-2)} (\psi_R^2(z) + \psi_L^2(z)) z^{-(j-2)} \right] \\ &= \frac{1}{2g_5^2} \frac{2^{2-\Delta(j)} \tilde{\kappa}_N^{j-2-\Delta(j)}}{\Gamma(\tilde{a}(j))} \int_0^1 dx x^{\tilde{a}(j)-1} (1-x)^{-\tilde{b}(j)} (I_z^R(x) + I_z^L(x)), \end{aligned} \quad (\text{E.3})$$

where the fermionic integrals are defined as ( $\xi = \tilde{\kappa}_N^2 z^2$ )

$$I_z^{R/L}(x) = \int dz \sqrt{g} e^{-\phi} z^{1+2(j-2)} \psi_{R/L}^2(z) \xi^{\frac{-(j-2)}{2}} \xi^{2-\frac{\Delta(j)}{2}} \exp\left(-\frac{2x\xi}{1-x}\right), \quad (\text{E.4})$$

and j-dependent parameters are

$$\begin{aligned} \tilde{a}(j) &= a_k + 2 - \frac{1}{2}\Delta(j) & \text{and} & & \tilde{b}(j) &= 3 - \Delta(j) \\ \Delta(j) &= 2 + \sqrt{2\sqrt{\lambda}(j-j_0)} & \text{and} & & j_0 &= 2 - \frac{2}{\sqrt{\lambda}} \end{aligned} \quad (\text{E.5})$$

Using the bulk Dirac wavefunctions (D.6) for the soft-wall model, we can further reduce the fermionic integrals (E.4) to have [52]

$$\begin{aligned} I_z^R(x) &= \frac{1}{2} \times \tilde{\kappa}_N^{-2(j-2)} \times \left(\frac{\tilde{n}_R}{\tilde{\kappa}_N^{\tau-1}}\right)^2 \times \Gamma\left(\frac{j-2}{2} + \tau - \frac{\Delta(j)}{2} + 1\right) \times \left(\frac{1+x}{1-x}\right)^{-\frac{j-2}{2} - \tau + \frac{\Delta(j)}{2} - 1}, \\ I_z^L(x) &= \frac{1}{2} \times \tilde{\kappa}_N^{-2(j-2)} \times \left(\frac{\tilde{n}_L}{\tilde{\kappa}_N^{\tau}}\right)^2 \times \Gamma\left(\frac{j-2}{2} + \tau - \frac{\Delta(j)}{2} + 2\right) \times \left(\frac{1+x}{1-x}\right)^{-\frac{j-2}{2} - \tau + \frac{\Delta(j)}{2} - 2}. \end{aligned} \quad (\text{E.6})$$

Using (E.6) in (E.3), the spin- $j$  form factor of the Dirac fermion reduces to

$$A(j, K) = \frac{1}{4g_5^2} \frac{\tilde{\kappa}_N^{-(j-2)-\Delta(j)}}{\Gamma(\tilde{a}(j))} \int_0^1 dx x^{\tilde{a}(j)-1} (1-x)^{-\tilde{b}(j)} \times \left( \left( \frac{\tilde{n}_R}{\tilde{\kappa}_N^{\tau-1}} \right)^2 \times \Gamma(c(j)) \left( \frac{1+x}{1-x} \right)^{-c(j)} + \left( \frac{\tilde{n}_L}{\tilde{\kappa}_N^\tau} \right)^2 \times \Gamma(c(j)+1) \left( \frac{1+x}{1-x} \right)^{-(c(j)+1)} \right), \quad (\text{E.7})$$

with  $\Delta(j)$ ,  $\tilde{a}(j)$ ,  $\tilde{b}(j)$  given in (E.5) and

$$c(j) = (\tau + 1) + \frac{j-2}{2} - \frac{\Delta(j)}{2} \quad (\text{E.8})$$

$A(j, K)$  is the spin- $j$  generalization of the spin-2 graviton form factor (D.7). The  $x$ -integral form (E.7) can be interpreted as the holographic *partonic* content of the Dirac fermion at strong coupling for spin- $j$ , with  $x$  playing the role of the Bjorken momentum fraction.

## Appendix F. Pomeron-Pomeron-gluon bulk coupling

The sphaleron at the boundary of the Witten vertex sources either  $G^2$  or  $G\tilde{G}$ .  $G^2$  is dual to the dilaton in bulk, while  $G\tilde{G}$  is dual to the axion, both of which are described by massive glueballs of even and odd parity respectively.  $G^2$  yields a direct scalar Pomeron-Pomeron-dilaton coupling times the pertinent bulk-to-boundary propagator.  $G\tilde{G}$  yields an indirect pseudoscalar Pomeron-Pomeron-pseudoscalar coupling by mixing to the bulk singlet and Chern-Simons term, times pertinent bulk-to-bulk and bulk-to-boundary propagators

### Appendix F.1. Bulk dilaton-graviton-graviton coupling

The graviton in bulk is dual to a scalar glueball or  $G^2$  on the boundary. The effective action for the graviton is given by the standard Einstein-Hilbert action

$$\frac{1}{2\tilde{g}_5^2} \int d^5x \sqrt{g} e^{-2\phi} \sqrt{R} \quad (\text{F.1})$$

with  $R$  the scalar curvature and  $2\tilde{g}_5^2 = 2\kappa^2 = 16\pi G_N = 8\pi^2/N_c^2$ . To extract the bulk gravitational coupling, we linearize the metric around the flat metric  $\eta_{\mu\nu} \rightarrow \eta_{\mu\nu} + \sqrt{2\kappa^2} h_{\mu\nu}$ . In de Donder gauge with  $\partial_\alpha h_\mu^\alpha = \frac{1}{2} \partial_\mu f$  and  $f = h_\mu^\mu$ , the expansion of (F.1) yields the quadratic contributions

$$(\sqrt{2\kappa^2})^2 \left( \frac{1}{8\tilde{g}_5^2} g^{MN} \eta^{\alpha\bar{\alpha}} \eta^{\beta\bar{\beta}} \partial_M h_{\alpha\bar{\alpha}} \partial_N h_{\beta\bar{\beta}} - \frac{1}{4\tilde{g}_5^2} g^{MN} \eta^{\alpha\bar{\alpha}} \eta^{\beta\bar{\beta}} \partial_M h_{\alpha\beta} \partial_N h_{\bar{\alpha}\bar{\beta}} \right) \quad (\text{F.2})$$

and the cubic contributions

$$(\sqrt{2\kappa^2})^3 \left( -\frac{1}{8\tilde{g}_5^2} g^{MN} \eta^{\alpha\bar{\alpha}} \eta^{\beta\bar{\beta}} f \partial_M h_{\alpha\bar{\alpha}} \partial_N h_{\beta\bar{\beta}} - \frac{1}{4\tilde{g}_5^2} g^{MN} \eta^{\alpha\bar{\alpha}} \eta^{\beta\bar{\beta}} \partial_M f h_{\alpha\bar{\alpha}} \partial_N h_{\beta\bar{\beta}} \right) \quad (\text{F.3})$$

where only the couplings through the traceful  $f$  and traceless  $h_{\alpha\beta}$  were retained. Note that  $f(z=0, x)$  couples to  $T_\mu^\mu(x)$  of the gauge theory on the boundary, hence the identification with the dual of  $G^2$ .

The induced interaction between the scalar and the graviton on the boundary, follows from the bulk decomposition  $h_{\mu\nu}(x, z) = h(z)h_{\mu\nu}(x)$  and  $f(x, z) = s(z)f(x)$ , in the form

$$\int d^4x \eta^{\alpha\bar{\alpha}} \eta^{\beta\bar{\beta}} \left( \begin{aligned} & \mathbf{C}_1^+ f(x) \eta^{\mu\nu} \partial_\mu h_{\alpha\bar{\beta}}(x) \partial_\nu h_{\bar{\alpha}\beta}(x) \\ & + \mathbf{C}_2^+ f(x) h_{\alpha\bar{\beta}}(x) h_{\bar{\alpha}\beta}(x) + \mathbf{C}_3^+ \eta^{\mu\nu} \partial_\mu f(x) h_{\alpha\bar{\beta}}(x) \partial_\nu h_{\bar{\alpha}\beta}(x) \end{aligned} \right) \quad (\text{F.4})$$

with the induced bulk coefficients

$$\begin{aligned} \mathbf{C}_1^+ &= -\frac{(\sqrt{2\kappa^2})^3}{4\tilde{g}_5^2} \int dz \sqrt{g} e^{-\phi} \left( \frac{z^2}{2} s(z) h^2(z) \right) \\ \mathbf{C}_2^+ &= +\frac{(\sqrt{2\kappa^2})^3}{4\tilde{g}_5^2} \int dz \sqrt{g} e^{-\phi} \left( \frac{z^2}{2} s(z) h'^2(z) + \frac{z^2}{2} s'(z) (h^2)'(z) \right) \\ \mathbf{C}_3^+ &= -\frac{(\sqrt{2\kappa^2})^3}{4\tilde{g}_5^2} \int dz \sqrt{g} e^{-\phi} \left( z^2 s(z) h^2(z) \right) \end{aligned} \quad (\text{F.5})$$

with  $2\tilde{g}_5^2 = 2\kappa^2 = 8\pi^2/N_c^2$ . For the Witten diagram in Fig. 10, we note that for a massive  $0^+$  production, the vertex is close to the boundary. If we denote by  $z_5 = z \approx 0$  the position of the vertex in bulk, each of the two bulk-to-bulk graviton propagators factors out

$$G(z \approx 0, z') \approx \frac{z^4}{4} \mathcal{H}(K, z') \approx h(z) \mathcal{H}(K, z') \quad (\text{F.6})$$

with  $\mathcal{H}(K, z')$  the non-normalizable bulk-to-boundary graviton propagator in (D.5). Finally, we identify  $s(z)$  with the normalizable scalar  $0^+$  glueball state in bulk. So the fields in (F.5) read

$$h(z) \approx \frac{z^4}{4} \quad s(z) \approx \mathcal{S}(M_{0^+}, z) \quad (\text{F.7})$$

### Appendix F.2. Bulk axion-graviton-graviton coupling

The boundary pseudoscalar glueball or  $G\tilde{G}$  is dual to the axion field  $a$  in bulk. We now note that the axion mixes with the flavor singlet U(1) gauge field  $A_M$  in bulk and the latter interacts with the bulk gravitons through the chiral-gravitational anomaly or Chern-Simons term [7]

$$\frac{N_c}{1536\pi^2} \int d^5x \sqrt{g} e^{-\phi} \epsilon^{MNPQR} g^{S\bar{S}} g^{T\bar{T}} \text{Tr} A_M R_{NPST} R_{QRT\bar{S}} \quad (\text{F.8})$$

with  $R_{NPST}$  the Riemann tensor. The mixing between the axion  $a$  and the scalar part of the singlet U(1) gauge field  $A_{M=z}$  that is consistent with the QCD  $U_A(1)$  axial anomaly can be captured in (F.8) through the minimal gauge shift  $A_z \rightarrow A_z + \partial_z a$ ,

$$\frac{N_f N_c}{1536\pi^2} \int d^5x \sqrt{g} e^{-\phi} \epsilon^{zNPQR} g^{S\bar{S}} g^{T\bar{T}} \partial_z a R_{NPST} R_{QRT\bar{S}} \quad (\text{F.9})$$

The coupling of the axion to the graviton follows by expanding the metric  $g_{MN} = \eta_{MN} + \delta_{\mu M} \delta_{\nu N} \sqrt{2\kappa^2} h_{\mu\nu}$ , with the result

$$\begin{aligned} \frac{N_f N_c \kappa^2}{764\pi^2} \int d^5x \sqrt{g} e^{-\phi} \epsilon^{\mu\nu\rho\sigma} \partial_z a & \left( \frac{9}{2} \eta^{\alpha\beta} \eta^{\gamma\delta} \partial_\mu h_{\nu\alpha} \partial_\sigma h_{\rho\beta} - 6\eta^{\alpha\beta} \partial_z \partial_\mu h_{\nu\alpha} \partial_\sigma h_{\rho\beta} \right. \\ & \left. + 2\eta^{\alpha\beta} \partial_z \partial_\mu h_{\nu\alpha} \partial_z \partial_\sigma h_{\rho\beta} + 2\eta^{\alpha\beta} \eta^{\gamma\delta} \partial_\gamma \partial_\mu h_{\nu\alpha} \partial_\sigma (\partial_\delta h_{\rho\beta} - \partial_\beta h_{\rho\delta}) \right) \end{aligned} \quad (\text{F.10})$$

Note that  $a(z=0, x)$  couples to the topological charge density or  $G\tilde{G}(x)$  of the gauge theory on the boundary. Using the bulk decomposition for the axion and the graviton

$$a_z(x, z) = \theta(z)a(x) \quad h_{\mu\nu}(x, z) = h(z)h_{\mu\nu}(x) \quad (\text{F.11})$$

(F.10) yields the boundary interaction

$$\int d^4x a(x) \left( \mathbf{C}_1^- \eta^{\alpha\beta} \eta^{\gamma\delta} \partial_\mu h_{\nu\alpha}(x) \partial_\sigma h_{\rho\beta}(x) + \mathbf{C}_2^- \eta^{\alpha\beta} \eta^{\gamma\delta} \partial_\gamma \partial_\mu h_{\nu\alpha}(x) \partial_\sigma (\partial_\delta h_{\rho\beta}(x) - \partial_\beta h_{\rho\delta}(x)) \right) \quad (\text{F.12})$$

with the induced coefficients

$$\begin{aligned} \mathbf{C}_1^- &= \frac{N_f N_c \kappa^2}{764\pi^2} \int dz \sqrt{g} e^{-\phi} \theta'(z) \left( \frac{9}{2} h^2(z) - 6hh'(z) + 2h'^2(z) \right) \\ \mathbf{C}_2^- &= \frac{N_f N_c \kappa^2}{764\pi^2} \int dz \sqrt{g} e^{-\phi} \theta'(z) h^2(z) \end{aligned} \quad (\text{F.13})$$

Again, for the Witten diagram in Fig. 10, we note that for a massive  $0^-$  production, the vertex is also close to the boundary. The same reasoning as in (F.6-F.7) shows that the bulk fields in (F.13) read

$$h(z) \approx \frac{z^4}{4} \quad \theta(z) \approx \mathcal{P}(M_{0^-, z}) \quad (\text{F.14})$$

where the latter refers to the normalized pseudo-scalar glueball state in bulk.

## Appendix G. Diffractive amplitudes

The use of Witten diagrams for DIS scattering in holographic QCD was pioneered by [5, 5]. In particular, the Pomeron was identified in bulk with a Reggeized graviton which transmutes to a string exchange. Numerous studies along these lines followed, which we cannot fully and fairly cover here. We only mention the original suggestion made in [50] and based on a holographic string exchange which triggered all these studies, and which ultimately identifies the holographic Pomeron exchange with a stringy instanton exchange [62]. In this Appendix, we use the Witten diagram approach as details how the Pomeron interacts in bulk, and follow the conventions detailed in [52]

### Appendix G.1. Amplitude for emitting a pseudo-scalar

For the Witten diagram with outgoing pseudo-scalar glueball  $X = G\tilde{G} = 0^-$ , the contribution is

$$\mathcal{A}_{pp \rightarrow pp 0^-}(j_1, j_2, s, t) = [\mathcal{V}_{h\Psi\Psi}^{\alpha\beta(TT)}(j_1, p_1, p_3, k_1)] \times [\mathbb{B}_{\alpha\beta\bar{\alpha}\bar{\beta}}^-(t_1, t_2, k_1, k_2)] \times [\mathcal{V}_{h\Psi\Psi}^{\bar{\alpha}\bar{\beta}(TT)}(j_2, p_2, p_4, k_2)] \quad (\text{G.1})$$

with  $k_1 = p_1 - p_3$  and  $k_2 = p_2 - p_4$  and  $t_{1,2} = -k_{1,2}^2$ , for spin  $j_{1,2}$  exchanges in the t-channel. The  $\mathbb{P}0^-$  vertex is

$$\mathbb{B}_{\alpha\beta\bar{\alpha}\bar{\beta}}^-(t_1, t_2, k_1, k_2) = (B_1^-(t_1, t_2)\eta_{\beta\bar{\beta}} + B_2^-(t_1, t_2)k_{2\beta}k_{1\bar{\beta}})\epsilon_{\alpha\bar{\alpha}\gamma\delta}k_1^\gamma k_2^\delta \quad (\text{G.2})$$

(G.2) is consistent with charge conjugation and Lorentz symmetries, and follows from the Chern-Simons vertex (F.12) after inserting the plane wave decomposition

$$a(x) = e^{-ip_5 x} \quad h_{\mu\nu}(x) = \epsilon_{\mu\nu}(k)e^{ik \cdot x} \quad (\text{G.3})$$

with the explicit vertex factors

$$B_1^-(t_1, t_2) = 2(\mathbf{C}_1^- - \mathbf{C}_2^- k_1 \cdot k_2) \quad B_2^-(t_1, t_2) = 2\mathbf{C}_2^- \quad (\text{G.4})$$

### Appendix G.2. Amplitude for emitting a scalar

For the Witten diagram with outgoing scalar glueball  $X = G^2 = 0+$ , the contribution is

$$\mathcal{A}_{pp \rightarrow pp0+}(j_1, j_2, s, t) = [\mathcal{V}_{h\Psi\Psi}^{\alpha\beta(TT)}(j_1, p_1, p_3, k_1)] \times [\mathbb{B}_{\alpha\beta\bar{\alpha}\bar{\beta}}^+(t_1, t_2, k_1, k_2)] \times [\mathcal{V}_{h\Psi\Psi}^{\bar{\alpha}\bar{\beta}(TT)}(j_2, p_2, p_4, k_2)] \quad (\text{G.5})$$

with the general scalar  $\mathbb{P}\mathbb{P}0+$  vertex for the process  $h(k_1) + h(k_2) \rightarrow f(p_5)$

$$\mathbb{B}_{\alpha\beta\bar{\alpha}\bar{\beta}}^+(t_1, t_2, k_1, k_2) = B^+(t_1, t_2, p_5^2) \eta_{\alpha\bar{\alpha}} \eta_{\beta\bar{\beta}} \quad (\text{G.6})$$

as quoted in (64). Note that (G.6) is consistent with parity, charge conjugation and Lorentz symmetries. More explicitly, for the fusion process  $h(k_1) + h(k_2) \rightarrow f(p_5)$  with

$$h_{\mu\nu}(x) = \epsilon_{\mu\nu}^{TT}(k) e^{+ik_{1,2} \cdot x} \quad f(x) = e^{-ip_5 \cdot x} \quad (\text{G.7})$$

and the transverse and traceless polarizations  $k^\mu \epsilon_{\mu\nu}^{TT}(k_{1,2}) = 0$  and  $\eta^{\mu\nu} \epsilon_{\mu\nu}^{TT}(k) = 0$ , (G.6) follows from the cubic graviton coupling (F.3).

### Appendix G.3. Reggeization

The Reggeized form of the amplitude (G.1) follows from the double Mellin transforms

$$\begin{aligned} & \mathcal{A}_{pp \rightarrow pp0-}(s_1, s_2, s, t) \\ &= \int_{\mathbb{C}_1} \frac{dj_1}{2\pi i} \left( \frac{s_1^{j_1-2} + (-s_1)^{j_1-2}}{\sin \pi j_1} \right) \int_{\mathbb{C}_2} \frac{dj_2}{2\pi i} \left( \frac{s_2^{j_2-2} + (-s_2)^{j_2-2}}{\sin \pi j_2} \right) \mathcal{A}_{pp \rightarrow pp0-}(j_1, j_2, s, t) \end{aligned} \quad (\text{G.8})$$

The contours  $\mathbb{C}_{1,2}$  are at the rightmost of the branch-points of  $A(j_{1,2}, k)$  as defined in (E.7). Each of the Mellin transform in (G.8) factorizes generically to

$$\int_{\mathbb{C}} \frac{dj}{2\pi i} \left( \frac{s^{j-2} + (-s)^{j-2}}{\sin \pi j} \right) A(j, k) \quad (\text{G.9})$$

The Pomeron amplitude follows by closing the contour to the left. The imaginary part follows from the discontinuity of the  $\Gamma$ -function in  $A(j, k)$  with the result

$$-\tilde{s}^{j_0} \int_{-\infty}^{j_0} \frac{dj}{\pi} \left( \frac{1 + e^{-i\pi}}{\sin \pi j} \right) \tilde{s}^{j-j_0} \sin \left[ \tilde{\xi} \sqrt{2\sqrt{\lambda}(j_0 - j)} \right] \frac{\kappa_N^{2j}}{s^2} \Gamma(\Delta(j) - 2) A(j, k) \Big|_{j \rightarrow j_0, \Delta(j) \rightarrow 2} \quad (\text{G.10})$$

with  $j_0 = 2 - 2/\sqrt{\lambda}$ , and the  $t$ -dependence set to zero in the exponent. It will be restored in the final result by inspection. We have set  $\tilde{s} \equiv s/\tilde{\kappa}_N^2$ , and defined  $\tilde{\xi} \equiv \gamma + \pi/2$  with Euler constant  $\gamma = 0.5772$ . In the high energy limit  $\sqrt{\lambda}/\tilde{\tau} \rightarrow 0$  with  $\tilde{\tau} \equiv \log \tilde{s}$ , the  $j$ -integration yields

$$e^{j_0 \tilde{\tau}} \left[ (\sqrt{\lambda}/\pi) + i \right] (\sqrt{\lambda}/2\pi)^{1/2} \tilde{\xi} \frac{e^{-\sqrt{\lambda}\tilde{\xi}^2/2\tilde{\tau}}}{\tilde{\tau}^{3/2}} \left( 1 + \mathcal{O}\left(\frac{\sqrt{\lambda}}{\tilde{\tau}}\right) \right) \times \frac{\kappa_N^{2j}}{s^2} \Gamma(\Delta(j) - 2) A(j, k) \Big|_{j \rightarrow j_0, \Delta(j) \rightarrow 2} \quad (\text{G.11})$$



#### Appendix G.4. Final amplitudes

Combining the above results in (G.1) gives for the pseudo-scalar glueball emission amplitude

$$\begin{aligned}
& \left[ \left[ (\sqrt{\lambda}/\pi) + i \right] (\sqrt{\lambda}/2\pi)^{1/2} \tilde{\xi} \frac{e^{-\sqrt{\lambda}\xi^2/2\tilde{\tau}_1}}{\tilde{\tau}_1^{3/2}} \frac{A(j_0, k_1)}{\tilde{s}_1^{2-j_0}} \left[ \frac{1}{2} \bar{u}(p_3) \gamma^{[\alpha} p^{\beta]} u(p_1) \right] \right] \\
& \times \left[ \mathbb{B}_{\alpha\beta\bar{\alpha}\bar{\beta}}^-(t_1, t_2, k_1, k_2) \right] \\
& \times \left[ \left[ (\sqrt{\lambda}/\pi) + i \right] (\sqrt{\lambda}/2\pi)^{1/2} \tilde{\xi} \frac{e^{-\sqrt{\lambda}\xi^2/2\tilde{\tau}_2}}{\tilde{\tau}_2^{3/2}} \frac{A(j_0, k_2)}{\tilde{s}_2^{2-j_0}} \left[ \frac{1}{2} \bar{u}(p_4) \gamma^{[\bar{\alpha}} \underline{p}^{\bar{\beta}]} u(p_2) \right] \right] \quad (G.12)
\end{aligned}$$

with  $p = (p_1 + p_3)/2$  and  $\underline{p} = (p_2 + p_4)/2$ . Similarly, combining the above results in (G.5) yields the scalar glueball emission amplitude

$$\begin{aligned}
& \left[ \left[ (\sqrt{\lambda}/\pi) + i \right] (\sqrt{\lambda}/2\pi)^{1/2} \tilde{\xi} \frac{e^{-\sqrt{\lambda}\xi^2/2\tilde{\tau}_1}}{\tilde{\tau}_1^{3/2}} \frac{A(j_0, k_1)}{\tilde{s}_1^{2-j_0}} \left[ \frac{1}{2} \bar{u}(p_3) \gamma^{[\alpha} p^{\beta]} u(p_1) \right] \right] \\
& \times \left[ \mathbb{B}_{\alpha\beta\bar{\alpha}\bar{\beta}}^+(t_1, t_2, k_1, k_2) \right] \\
& \times \left[ \left[ (\sqrt{\lambda}/\pi) + i \right] (\sqrt{\lambda}/2\pi)^{1/2} \tilde{\xi} \frac{e^{-\sqrt{\lambda}\xi^2/2\tilde{\tau}_2}}{\tilde{\tau}_2^{3/2}} \frac{A(j_0, k_2)}{\tilde{s}_2^{2-j_0}} \left[ \frac{1}{2} \bar{u}(p_4) \gamma^{[\bar{\alpha}} \underline{p}^{\bar{\beta}]} u(p_2) \right] \right] \quad (G.13)
\end{aligned}$$

#### References

- [1] E. Shuryak, I. Zahed, Semiclassical double pomeron production of glueballs and eta-prime, Phys. Rev. D 68 (2003) 034001. [arXiv:hep-ph/0302231](#), doi:10.1103/PhysRevD.68.034001.
- [2] A. Kirk, et al., New effects observed in central production by the WA102 experiment at the CERN Omega spectrometer, in: 28th International Symposium on Multiparticle Dynamics (ISMD 98), 1998. [arXiv:hep-ph/9810221](#).
- [3] A. Brandt, S. Erhan, A. Kuzucu, M. Medinnis, N. Ozdes, P. E. Schlein, M. T. Zeyrek, J. G. Zweizig, J. B. Cheze, J. Zembery, A Study of inclusive double pomeron exchange in  $p\bar{p} \rightarrow pX\bar{p}$  at  $\sqrt{s} = 630$ -GeV, Eur. Phys. J. C 25 (2002) 361–377. [arXiv:hep-ex/0205037](#), doi:10.1007/s10052-002-1031-x.
- [4] O. Suranyi, Recent CMS and CMS-TOTEM results on diffraction and exclusive production, in: 18th Conference on Elastic and Diffractive Scattering, 2020. [arXiv:2002.06959](#).
- [5] J. Polchinski, M. J. Strassler, Deep inelastic scattering and gauge / string duality, JHEP 05 (2003) 012. [arXiv:hep-th/0209211](#), doi:10.1088/1126-6708/2003/05/012.
- [6] R. C. Brower, J. Polchinski, M. J. Strassler, C.-I. Tan, The Pomeron and gauge/string duality, JHEP 12 (2007) 005. [arXiv:hep-th/0603115](#), doi:10.1088/1126-6708/2007/12/005.
- [7] N. Anderson, S. K. Domokos, J. A. Harvey, N. Mann, Central production of  $\eta$  and  $\eta$ -prime via double Pomeron exchange in the Sakai-Sugimoto model, Phys. Rev. D 90 (8) (2014) 086010. [arXiv:1406.7010](#), doi:10.1103/PhysRevD.90.086010.
- [8] I. Iatrakis, A. Ramamurti, E. Shuryak, Pomeron Interactions from the Einstein-Hilbert Action, Phys. Rev. D 94 (4) (2016) 045005. [arXiv:1602.05014](#), doi:10.1103/PhysRevD.94.045005.
- [9] C. Ewerz, P. Lebiedowicz, O. Nachtmann, A. Szczurek, Helicity in proton–proton elastic scattering and the spin structure of the pomeron, Phys. Lett. B 763 (2016) 382–387. [arXiv:1606.08067](#), doi:10.1016/j.physletb.2016.10.064.

- [10] E. A. Kuraev, L. N. Lipatov, V. S. Fadin, Multi - Reggeon Processes in the Yang-Mills Theory, *Sov. Phys. JETP* 44 (1976) 443–450.
- [11] G. Basar, D. E. Kharzeev, H.-U. Yee, I. Zahed, Holographic Pomeron and the Schwinger mechanism, *PoS QNP2012* (2012) 116. doi:10.22323/1.157.0116.
- [12] D. M. Ostrovsky, G. W. Carter, E. V. Shuryak, Forced tunneling and turning state explosion in pure Yang-Mills theory, *Phys. Rev. D* 66 (2002) 036004. arXiv:hep-ph/0204224, doi:10.1103/PhysRevD.66.036004.
- [13] F. R. Klinkhamer, N. S. Manton, A Saddle Point Solution in the Weinberg-Salam Theory, *Phys. Rev. D* 30 (1984) 2212. doi:10.1103/PhysRevD.30.2212.
- [14] V. V. Khoze, A. Ringwald, Valley trajectories in gauge theories.
- [15] E. V. Shuryak, J. J. M. Verbaarschot, On baryon number violation and nonperturbative weak processes at SSC energies, *Phys. Rev. Lett.* 68 (1992) 2576–2579. doi:10.1103/PhysRevLett.68.2576.
- [16] E. V. Shuryak, I. Zahed, Instanton induced effects in QCD high-energy scattering, *Phys. Rev. D* 62 (2000) 085014. arXiv:hep-ph/0005152, doi:10.1103/PhysRevD.62.085014.
- [17] M. A. Nowak, E. V. Shuryak, I. Zahed, Instanton induced inelastic collisions in QCD, *Phys. Rev. D* 64 (2001) 034008. arXiv:hep-ph/0012232, doi:10.1103/PhysRevD.64.034008.
- [18] I. I. Balitsky, A. V. Yung, Collective - Coordinate Method for Quasizero Modes, *Phys. Lett. B* 168 (1986) 113–119. doi:10.1016/0370-2693(86)91471-1.
- [19] E. V. Shuryak, Toward the Quantitative Theory of the 'Instanton Liquid' 4. Tunneling in the Double Well Potential, *Nucl. Phys. B* 302 (1988) 621–644. doi:10.1016/0550-3213(88)90191-5.
- [20] A. V. Yung, Instanton Vacuum in Supersymmetric QCD, *Nucl. Phys. B* 297 (1988) 47. doi:10.1016/0550-3213(88)90199-X.
- [21] J. J. M. Verbaarschot, Streamlines and conformal invariance in Yang-Mills theories, *Nucl. Phys. B* 362 (1991) 33–53, [Erratum: *Nucl.Phys.B* 386, 236–236 (1992)]. doi:10.1016/0550-3213(91)90554-B.
- [22] E. Shuryak, I. Zahed, Prompt quark production by exploding sphalerons, *Phys. Rev. D* 67 (2003) 014006. arXiv:hep-ph/0206022, doi:10.1103/PhysRevD.67.014006.
- [23] M. Luscher, SO(4) Symmetric Solutions of Minkowskian Yang-Mills Field Equations, *Phys. Lett. B* 70 (1977) 321–324. doi:10.1016/0370-2693(77)90668-2.
- [24] B. M. Schechter, Yang-Mills Theory on the Hypertorus, *Phys. Rev. D* 16 (1977) 3015. doi:10.1103/PhysRevD.16.3015.
- [25] A. Hasenfratz, Spatial correlation of the topological charge in pure SU(3) gauge theory and in QCD, *Phys. Lett. B* 476 (2000) 188–192. arXiv:hep-lat/9912053, doi:10.1016/S0370-2693(00)00105-2.
- [26] E. V. Shuryak, Probing the boundary of the nonperturbative QCD by small size instantons arXiv:hep-ph/9909458.
- [27] E. V. Shuryak, The Role of Instantons in Quantum Chromodynamics. 1. Physical Vacuum, *Nucl. Phys. B* 203 (1982) 93. doi:10.1016/0550-3213(82)90478-3.
- [28] A. Ramamurti, E. Shuryak, I. Zahed, Are there monopoles in the quark-gluon plasma?, *Phys. Rev. D* 97 (11) (2018) 114028. arXiv:1802.10509, doi:10.1103/PhysRevD.97.114028.
- [29] T. Schäfer, E. V. Shuryak, Instantons in QCD, *Rev. Mod. Phys.* 70 (1998) 323–426. arXiv:hep-ph/9610451, doi:10.1103/RevModPhys.70.323.

- [30] R. D. Pisarski, L. G. Yaffe, THE DENSITY OF INSTANTONS AT FINITE TEMPERATURE, *Phys. Lett. B* 97 (1980) 110–112. doi:10.1016/0370-2693(80)90559-6.
- [31] E. V. Shuryak, M. Velkovsky, The Instanton density at finite temperatures, *Phys. Rev. D* 50 (1994) 3323–3327. arXiv:hep-ph/9403381, doi:10.1103/PhysRevD.50.3323.
- [32] D. B. Leinweber, Visualizations of the QCD vacuum, in: *Workshop on Light-Cone QCD and Nonperturbative Hadron Physics*, 1999, pp. 138–143. arXiv:hep-lat/0004025.
- [33] J. D. Bjorken, Intersections 2000: What’s new in hadron physics, *AIP Conf. Proc.* 549 (1) (2000) 211–229. arXiv:hep-ph/0008048, doi:10.1063/1.1345244.
- [34] V. Zetocha, T. Schäfer, Instanton contribution to scalar charmonium and glueball decays, *Phys. Rev. D* 67 (2003) 114003. arXiv:hep-ph/0212125, doi:10.1103/PhysRevD.67.114003.
- [35] S. Chernyshev, M. A. Nowak, I. Zahed, Heavy hadrons and QCD instantons, *Phys. Rev. D* 53 (1996) 5176–5184. arXiv:hep-ph/9510326, doi:10.1103/PhysRevD.53.5176.
- [36] M. A. Nowak, M. Rho, I. Zahed, *Chiral nuclear dynamics*, 1996.
- [37] S. Chernyshev, M. A. Nowak, I. Zahed, Heavy hadrons and QCD instantons, *Phys. Rev. D* 53 (1996) 5176–5184. arXiv:hep-ph/9510326, doi:10.1103/PhysRevD.53.5176.
- [38] F. Sauter, Über das Verhalten eines Elektrons im homogenen elektrischen Feld nach der relativistischen Theorie Diracs, *Z. Phys.* 69 (1931) 742–764. doi:10.1007/BF01339461.
- [39] D. E. Kharzeev, The Chiral Magnetic Effect and Anomaly-Induced Transport, *Prog. Part. Nucl. Phys.* 75 (2014) 133–151. arXiv:1312.3348, doi:10.1016/j.pnpnp.2014.01.002.
- [40] P. Faccioli, Instanton contribution to the electromagnetic form-factors of the nucleon, *Phys. Rev. C* 69 (2004) 065211. arXiv:hep-ph/0312019, doi:10.1103/PhysRevC.69.065211.
- [41] P. V. Buividovich, M. N. Chernodub, E. V. Luschevskaya, M. I. Polikarpov, Numerical study of chiral symmetry breaking in non-Abelian gauge theory with background magnetic field, *Phys. Lett. B* 682 (2010) 484–489. arXiv:0812.1740, doi:10.1016/j.physletb.2009.11.017.
- [42] G. Basar, G. V. Dunne, D. E. Kharzeev, Electric dipole moment induced by a QCD instanton in an external magnetic field, *Phys. Rev. D* 85 (2012) 045026. arXiv:1112.0532, doi:10.1103/PhysRevD.85.045026.
- [43] A. Ringwald, F. Schrempp, Instanton induced cross-sections in deep inelastic scattering, *Phys. Lett. B* 438 (1998) 217–228. arXiv:hep-ph/9806528, doi:10.1016/S0370-2693(98)00953-8.
- [44] V. V. Khoze, F. Krauss, M. Schott, Large Effects from Small QCD Instantons: Making Soft Bombs at Hadron Colliders, *JHEP* 04 (2020) 201. arXiv:1911.09726, doi:10.1007/JHEP04(2020)201.
- [45] A. H. Mueller, On higher order semiclassical corrections to high-energy cross-sections in the one instanton sector, *Nucl. Phys. B* 364 (1991) 109–126. doi:10.1016/0550-3213(91)90580-Q.
- [46] V. Andreev, et al., Search for QCD instanton-induced processes at HERA in the high-  $Q^2$  domain, *Eur. Phys. J. C* 76 (7) (2016) 381. arXiv:1603.05567, doi:10.1140/epjc/s10052-016-4194-6.
- [47] A. M. Sirunyan, et al., Search for black holes and sphalerons in high-multiplicity final states in proton-proton collisions at  $\sqrt{s} = 13$  TeV, *JHEP* 11 (2018) 042. arXiv:1805.06013, doi:10.1007/JHEP11(2018)042.
- [48] F. L. Bezrukov, D. Levkov, C. Rebbi, V. A. Rubakov, P. Tinyakov, Suppression of baryon number violation in electroweak collisions: Numerical results, *Phys. Lett. B* 574 (2003) 75–81. arXiv:hep-ph/0305300, doi:10.1016/j.physletb.2003.09.015.

- [49] V. Khachatryan, et al., Exclusive and semi-exclusive  $\pi^+\pi^-$  production in proton-proton collisions at  $\sqrt{s} = 7$  TeV [arXiv:1706.08310](#).
- [50] M. Rho, S.-J. Sin, I. Zahed, Elastic parton-parton scattering from AdS / CFT, *Phys. Lett. B* 466 (1999) 199–205. [arXiv:hep-th/9907126](#), [doi:10.1016/S0370-2693\(99\)01118-1](#).
- [51] R. Brower, M. Djuric, C.-I. Tan, Holographic double diffraction of Higgs and the AdS/CFT graviton/Pomeron, *Int. J. Mod. Phys. A* 29 (28) (2014) 1446013. [arXiv:1412.3060](#), [doi:10.1142/S0217751X14460130](#).
- [52] K. A. Mamo, I. Zahed, Diffractive photoproduction of  $J/\psi$  and  $\Upsilon$  using holographic QCD: gravitational form factors and GPD of gluons in the proton, *Phys. Rev. D* 101 (8) (2020) 086003. [arXiv:1910.04707](#), [doi:10.1103/PhysRevD.101.086003](#).
- [53] P. E. Shanahan, W. Detmold, Gluon gravitational form factors of the nucleon and the pion from lattice QCD, *Phys. Rev. D* 99 (1) (2019) 014511. [arXiv:1810.04626](#), [doi:10.1103/PhysRevD.99.014511](#).
- [54] W. Xiong, et al., A small proton charge radius from an electron–proton scattering experiment, *Nature* 575 (7781) (2019) 147–150. [doi:10.1038/s41586-019-1721-2](#).
- [55] V. A. Khoze, V. V. Khoze, D. L. Milne, M. G. Ryskin, Hunting for QCD Instantons at the LHC in Events with Large Rapidity Gaps [arXiv:2104.01861](#).
- [56] D. Kharzeev, E. Shuryak, I. Zahed, Sphalerons, baryogenesis, and helical magnetogenesis in the electroweak transition of the minimal standard model, *Phys. Rev. D* 102 (7) (2020) 073003. [arXiv:1906.04080](#), [doi:10.1103/PhysRevD.102.073003](#).
- [57] M. A. Nowak, J. J. M. Verbaarschot, I. Zahed, Flavor Mixing in the Instanton Vacuum, *Nucl. Phys. B* 324 (1989) 1–33. [doi:10.1016/0550-3213\(89\)90178-8](#).
- [58] Z. Abidin, C. E. Carlson, Nucleon electromagnetic and gravitational form factors from holography, *Phys. Rev. D* 79 (2009) 115003. [arXiv:0903.4818](#), [doi:10.1103/PhysRevD.79.115003](#).
- [59] S. Hong, S. Yoon, M. J. Strassler, On the couplings of vector mesons in AdS / QCD, *JHEP* 04 (2006) 003. [arXiv:hep-th/0409118](#), [doi:10.1088/1126-6708/2006/04/003](#).
- [60] Z. Abidin, C. E. Carlson, Gravitational form factors of vector mesons in an AdS/QCD model, *Phys. Rev. D* 77 (2008) 095007. [arXiv:0801.3839](#), [doi:10.1103/PhysRevD.77.095007](#).
- [61] C. A. Ballon Bayona, H. Boschi-Filho, N. R. F. Braga, Deep inelastic scattering from gauge string duality in the soft wall model, *JHEP* 03 (2008) 064. [arXiv:0711.0221](#), [doi:10.1088/1126-6708/2008/03/064](#).
- [62] G. Basar, D. E. Kharzeev, H.-U. Yee, I. Zahed, Holographic Pomeron and the Schwinger Mechanism, *Phys. Rev. D* 85 (2012) 105005. [arXiv:1202.0831](#), [doi:10.1103/PhysRevD.85.105005](#).